Acta Pharmaceutica Sinica B 2021;11(6):1648–1666

Chinese Pharmaceutical Association
Institute of Materia Medica, Chinese Academy of Medical Sciences

Acta Pharmaceutica Sinica B

www.elsevier.com/locate/apsb
www.sciencedirect.com

ORIGINAL ARTICLE

New guaiane-type sesquiterpenoid dimers from *Artemisia atrovirens* and their antihepatoma activity

Lihua Su[a,b], Xintian Zhang[a,b], Yunbao Ma[a], Changan Geng[a], Xiaoyan Huang[a], Jing Hu[a], Tianze Li[a], Shuang Tang[a,b], Cheng Shen[a,b], Zhen Gao[a,b], Xuemei Zhang[a], Ji-Jun Chen[a,b,*]

[a]*State Key Laboratory of Phytochemistry and Plant Resources in West China, Kunming Institute of Botany, Chinese Academy of Sciences, Yunnan Key Laboratory of Natural Medicinal Chemistry, Kunming 650201, China*
[b]*University of Chinese Academy of Sciences, Beijing 100049, China*

Received 26 September 2020; received in revised form 15 November 2020; accepted 7 December 2020

KEY WORDS

Guaianolide dimers;
Artematrolides A–R;
Artemisia atrovirens;
Cytotoxicity;
Cell cycle;
Apoptosis

Abstract Leading by cytotoxicity against HepG2 cells, bioactivity-guided fractionation of the EtOAc fraction from *Artemisia atrovirens* led to the isolation of 18 new guaianolide dimers, artematrolides A–R and lavandiolides A, B, C, H, and J. Eight compounds (**1**, **4**, **10**, **12**, **13**, and **19**–**21**) were unambiguously confirmed by the single-crystal X-ray diffraction analyses, and the others were elucidated based on IR, UV, HRESIMS, 1D and 2D NMR experiments, and comparison of the experimental and calculated ECD data. Structurally, all of them were [4 + 2] Diels–Alder adducts of two monomeric guaianolides. The isolates were evaluated for their cytotoxicity against three human hepatoma cell lines, and 19 compounds demonstrated cytotoxicity against HepG2, SMMC-7721, and Huh7 cell lines. Especially, compounds **1**, **12**, **14**, and **15** exhibited cytotoxicity with IC_{50} values of 4.4, 3.8, 7.6, and 6.7 μmol/L (HepG2), 9.6, 4.6, 6.6, and 6.0 μmol/L (SMMC-7721), and 7.6, 4.5, 6.9, and 5.6 μmol/L (Huh7), respectively. Notably, compound **12** showed the most promising activity against three human hepatoma cell lines and dose-dependently inhibited cell migration and invasion, induced G2/M cell cycle arrest and cell apoptosis in HepG2 cells, down-regulated the expression of BCL-2 and PARP-1, and activated PARP-1 to up-regulate the expression of cleaved-PARP-1.

*Corresponding author. Tel.: +86 871 65223265; fax: +86 871 65227197.
E-mail address: chenjj@mail.kib.ac.cn (Ji-Jun Chen).

Peer review under responsibility of Chinese Pharmaceutical Association and Institute of Materia Medica, Chinese Academy of Medical Sciences.

https://doi.org/10.1016/j.apsb.2020.12.006

1. Introduction

Hepatocellular carcinoma (HCC) is the major type of primary liver cancer and the third leading cause of cancer-related deaths worldwide[1,2]. Accumulating evidence suggests that HCC threatens people's heath more and more seriously, and the primary liver cancer incidence is still on the rise at the global level[3−5]. Although seven antihepatoma drugs including sorafenib, regorafenib, lenvatinib, cabozantinib, nivolumab, pembrolizumab, and ramucirumab are effectively therapeutic agents clinically, there are still disadvantages involving the low response rate, serious side effects, and drug resistance. Therefore, it is desirable to search the new and effective drugs against human hepatoma. Sesquiterpenoids and their dimers are reported to exhibit diverse activities[6−9], such as antitumor, antiinflammation, antimalaria, neurotrophic, etc., which are a group of effective and low-toxicity natural small molecules[10−13]. Guaianolide dimers are a class of intriguing sesquiterpenoid dimers predominantly in Asteraceae and Chloranthaceae families, especially in the *Artemisia* species[14]. The genus *Artemisia* (Asteraceae) includes about 380 species distributed all over the world, and 186 species in China[15]. Some species from the genus *Artemisia*, such as *A. annua*, *A. argyi*, *A. capillaris*, *A. scoparia*, and *A. anomala*, are used as the famous traditional Chinese medicinal herbs to treat a variety of diseases including malaria, hepatitis, cancer, eczema, diarrhea, bruise, and rheumatic disease and so on[16,17]. Up to now, a lot of *Artemisia* species had been phytochemically investigated to conclude that plants of the *Artemisia* genus were rich in sesquiterpenoids, especially guaianolides and their dimers[18−24], and 77 dimeric guaianolides had been reported from the *Artemisia* plants in last 40 years, including 19 ones from *A. argyi*[17,18,25−27], 11 ones from *A. absinthium*[23,28−32], 11 ones from *A. anomala*[20,33−35], six ones from *A. rupestris*[36], five ones from *A. sieversiana*[21,37], five ones from *A. caruifolia*[38], artemyriantholides A−D from *A. myriantha*[19], arteminolide and 8-acetylarteminolide from *A. sylvatica*[24,39], artselenoide from *A. selengensis*[40], artelein from *A. leucodes*[41], and lavandiolides A–L from *A. lavandulifolia*[42]. Based on the connecting model of the two monomeric sesquiterpenoid units, these dimeric guaianolides are classified as Diels−Alder, [2 + 2] cycloaddition, and ester linkage adducts (Supporting Information Table S1). Biogenetically, 71 dimers are derived from [4 + 2] cycloaddition of two guaiane moieties, while artelein and artesin A are formed *via* tandem [2 + 2]/[2 + 2] cycloadditions, and artemisianes A−D are condensed through esterification of two monomeric units. Interestingly, guaianolide-type dimers from the genus *Artemisia* species exhibited antitumor, antiinflammation, antivirus activities and so on. Artanomadimers A and F manifested cytotoxicity against the BGC-823 tumor cell line with IC_{50} values of 2.7 and 6.3 μmol/L[35]. Arteminolides A−D and 8-acetylarteminolide inhibited the farnesyl protein transferase (FPTase) with IC_{50} values of 0.7−1.0[25] and 1.8 μmol/L[39]. Artemisian B exhibited antiproliferative activity *via* apoptosis induction and G2/M arrest in MDA-MB-468 cells with an IC_{50} value of 3.2 μmol/L[18]. Artemisianin A displayed cytotoxicity against HT-29 cells with an IC_{50} value of 7.2 μmol/L and mediated cell apoptosis[27]. Absinthin C and isoanabsinthin showed inhibitory effects on LPS-induced NO production in BV-2 cells with IC_{50} values of 1.5 and 2.0 μmol/L[32]. Artemisianes A−D and lavandiolides A, C, G, and I demonstrated inhibitory activity on LPS-induced NO production in RAW 264.7 cells with IC_{50} values ranging from 0.6 to 32.1 μmol/L[12,42]. Caruifolin B showed anti-HIV activity by inhibiting the HIV-1-induced cytopathic effect in MT cells at 500 μg/mL[38]. Prompted by the diverse activities and intricate structures of guaianolide dimers in *Artemisia* species, phytochemical and biological investigation on this genus is an attractive topic.

To investigate structurally novel and bioactive dimeric sesquiterpenoids from natural plants, our assay suggested that the EtOH extract of *A. atrovirens* exhibited cytotoxicity against HepG2 cells with the inhibitory ratio of 98.9% at the concentration of 100.0 μg/mL. Previous report on essential oils from *A. atrovirens* by GC−MS analysis revealed its main constituents as 1,3-cyclopentadiene,5-(1,1-dimethylethyl), azulen-2-ol,1,4-dimethyl-7-(1-methylethyl), and eucalyptol, but no active compounds from *A. atrovirens* have been reported so far[43]. In our endeavor to search for novel and antihepatoma compounds from this species, 18 new guaianolide dimers and five known compounds lavandiolides A (**3**), B (**4**), C (**23**), H (**12**), and J (**9**), were isolated and identified with a spiro-system composed of two monomeric sesquiterpene lactone units. These five known compounds were just reported by Ye et al.[42] from *A. lavandulifolia* during the revision of this manuscript. Nineteen compounds showed cytotoxicity, and notably four compounds (**1**, **12**, **14**, and **15**) demonstrated significant cytotoxicity against three human hepatoma cell lines (HepG2, SMMC-7721, and Huh7). Herein, we described their isolation, structural elucidation, cytotoxicity, and the preliminary mechanism of the most active lavandiolide H (**12**).

2. Results and discussion

The EtOH extracts of the leaves of *A. atrovirens* were partitioned between EtOAc and H_2O. The active EtOAc fraction was subjected to silica gel, MCI gel CHP 20P, Sephadex LH-20, preparative HPLC, and semi-preparative HPLC to afford 23 sesquiterpenoid dimers (Fig. 1). The structures of artematrolides A−R (**1**, **2**, **5**−**8**, **10**, **11**, **13**−**22**) including their absolute configurations, were elucidated based on analyses of HRESIMS, 1D/2D NMR, ECD spectra, and single-crystal X-ray diffraction techniques.

Artematrolide A (**1**) was obtained as colorless orthorhombic crystals with a molecular formula of $C_{30}H_{36}O_6$ as inferred from its (+)-HRESIMS ion at *m/z* 515.2411 $[M+Na]^+$ (Calcd. for 515.2404), suggesting 13 degrees of unsaturation. Its IR spectrum displayed characteristic absorption bands assignable to hydroxy (3476 cm^{-1}), ester carbonyl (1767 and 1744 cm^{-1}), and olefinic (1629 cm^{-1}) functional groups. The ^1H NMR spectrum (Table 1) of compound **1** exhibited four singlet methyls at δ_H 1.26 (3H, s), 1.34 (3H, s), 1.50 (3H, s), and 1.92 (3H, s), two oxygenated methines at δ_H 5.24 (1H, d, $J=9.6$ Hz) and 4.38 (1H, dd, $J=10.2$, 10.2 Hz), and three olefinic protons at δ_H 6.18 (1H, d, $J=3.3$ Hz),

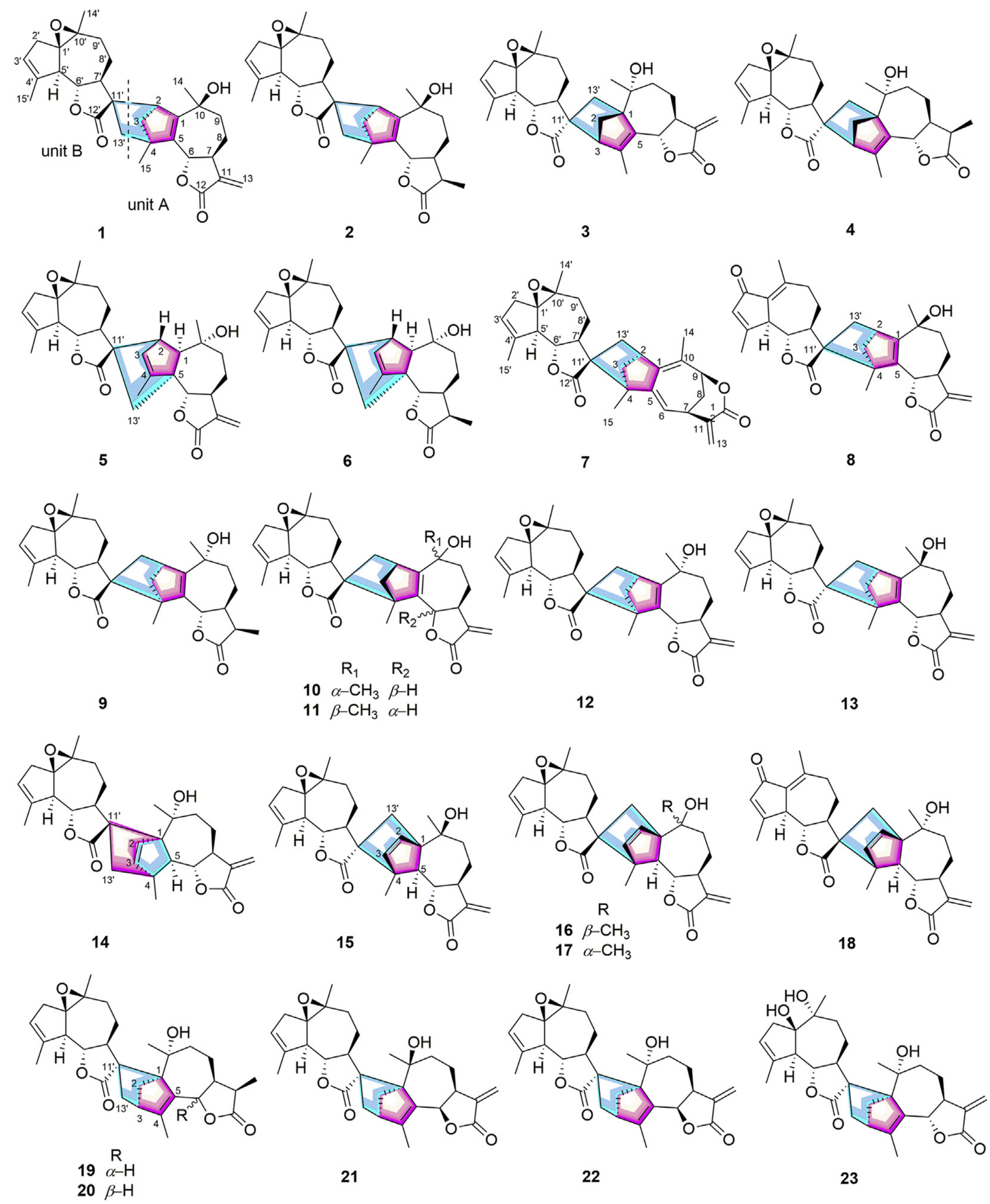

Figure 1 The structures of compounds **1**−**23**.

5.46 (1H, d, $J=3.3$ Hz), and 5.56 (1H, m). Its ^{13}C NMR spectrum (Table 4) revealed the presence of 30 carbons classified as four methyls, eight methylenes, seven methines, and 11 nonprotonated carbons. Among these carbons, two ester carbonyls at δ_C 183.6 and 170.2, and six olefinic carbons at δ_C 148.6, 144.9, 140.9, 139.9, 125.2, and 119.4 were easily recognized in the deshielded region. The abovementioned NMR and MS features suggested a dimeric sesquiterpenoid for compound **1**.

The planar structure of **1** involving units A and B was mainly accomplished by analyzing the 2D NMR data (Fig. 2). The $^1H-^1H$ COSY spectrum revealed four isolated spin-coupling systems of H-6/H-7/H_2-8/H_2-9, H-2/H_2-3, H-6′/H-7′/H_2-8′/H_2-9′, and H_2-2′/H-3′. The HMBC spectrum showed correlations from H_2-13 to C-7, C-11, and C-12, from H_3-14 to C-1, C-9, and C-10, from H_3-15 to C-3, C-4, and C-5, from H-8 to C-6, C-10, and C-11, and from H-2 to C-1, C-3, C-4, and C-5 in unit A; and correlations from H_3-14′ to C-1′, C-9′, and C-10′, from H_3-15′ to C-3′, C-4′, and C-5′, from H-7′ to C-5′, C-6′, C-8′, C-9′, C-12′, and C-13′, and from H_2-13′ to C-7′, C-11′, and C-12′ in unit B. From the above analyses, both units A and B were deduced as guaianolide-like moieties similar to arglabin[19]. The linkage of units A and B through two C−C single bonds of C-2−C-11′ and C-4−C-13′ was established by the key HMBC correlations of H_2-13′ with C-3, C-4, C-5, and C-15, of H-2 with C-7′, C-11′, C-12′, and C-13′, of H-3 with C-11′ and C-13′, and of H_3-15 with C-13′.

The relative configuration of **1** was determined by interpretation of ROESY spectrum (Fig. 3) and coupling constants. With the fact that H-7 of guaiane-type sesquiterpenoids always maintained

Table 1 ^{1}H NMR spectroscopic data for compounds **1**, **2**, and **5**–**8** (δ in ppm, J in Hz).

No. position	**1**[a,c]	**2**[a,c]	**5**[b,d]	**6**[b,d]	**7**[a,c]	**8**[b,d]
1			2.34 br s	2.33 br s		
2	3.24 br s	3.20 br s	3.25 m	3.23 m	3.06 m	3.04 m
3	1.46 dd (9.0, 1.8)	1.44 m	5.44 br s	5.42 br s	2.53 dd (9.6, 1.5)	1.58 m
	1.35 m	1.33 m			1.14 m	1.39 m
6	5.24 d (9.6)	5.28 d (9.6)	4.56 d (10.0)	4.76 d (11.2)	5.75 d (8.4)	5.56 (overlapped)
7	2.85 m	1.90 m	2.94 m	2.51 m	3.54 m	2.96 m
8	2.11 m	1.94 (overlapped)	2.23 m	1.86 (overlapped)	2.58 m	2.25 m
	1.88 m	1.87 m	1.44 m	1.43 m	1.94 m	1.73 m
9	2.00 (overlapped)	1.94 (overlapped)	1.81 m	1.75 m	4.94 dd (5.4, 1.8)	2.00 m
	1.70 m	1.61 m	1.64 m	1.54 m		1.83 m
11		2.24 m		2.71 m		
13	6.18 d (3.3)	1.22 (overlapped)	6.22 d (3.2)	1.23 d (8.0)	6.38 br s	6.11 d (3.6)
	5.46 d (3.3)		5.68 d (3.2)		5.54 br s	5.57 (overlapped)
14	1.26 s	1.22 (overlapped)	1.06 s	1.04 s	2.03 s	1.42 s
15	1.50 s	1.47 s	1.84 s	1.84 s	1.14 s	1.50 s
2′	2.75 m	2.75 br s	2.82 m	2.82 m	2.74 m	
	2.18 (overlapped)	2.16 (overlapped)	2.14 m	2.14 m	2.11 m	
3′	5.56 m	5.57 br s	5.60 m	5.60 m	5.56 m	6.16 s
5′	2.79 m	2.79 d (10.2)	2.88 m	2.88 m	2.81 d (10.5)	3.70 d (10.0)
6′	4.38 dd (10.2, 10.2)	4.37 dd (10.2, 10.2)	4.30 dd (10.4, 10.0)	4.29 dd (10.4, 10.0)	3.85 dd (10.5, 10.2)	3.65 dd (10.0, 9.6)
7′	1.78 m	1.77 m	1.94 (overlapped)	1.93 m	1.34 m	2.70 m
8′	1.61 m	1.61 m	1.87 m	1.87 (overlapped)	1.27 m	1.98 m
	1.57 m	1.57 m	1.67 m	1.68 m	1.20 m	1.58 m
9′	2.18 (overlapped)	2.17 (overlapped)	2.22 m	2.22 m	2.00 m	2.65 m
	1.91 m	1.89 m	2.03 m	2.04 m	1.79 m	2.35 m
13′	1.99 (overlapped)	1.97 m	1.76 d (12.4)	1.72 m	1.92 m	2.21 m
	1.39 d (12.0)	1.36 m	1.70 m	1.65 m	1.65 m	1.61 m
14′	1.34 s	1.34 s	1.34 s	1.34 s	1.31 s	2.42 s
15′	1.92 s	1.93 s	1.94 (overlapped)	1.94 s	1.93 s	2.33 s

[a]Recorded in $CDCl_3$. [b]Recorded in CD_3OD. [c]Recorded at 600 MHz. [d]Recorded at 400 MHz.

the α-orientation[37,44,45], the large coupling constant between H-6 and H-7 (J = 9.6 Hz) inferred that they were in the *anti*-axial configuration, *i.e.*, H-6 was assigned to be β-orientated[46]. In the ROESY spectrum, the cross peaks of H-7/H-3/H_3-14 indicated that CH_2-3 and CH_3-14 were α-orientated. Similarly, the ROESY correlation of H-7′ with H-5′ and the large coupling constant ($J_{H\text{-}6'/H\text{-}7'}$ = 10.2 Hz) assigned the α-orientation of H-5′ and H-7′ and β-orientation of H-6′. To our delight, suitable crystals of compound **1** were obtained from an optimized solvent system (MeOH−CH_2Cl_2, 10:90, *v*/*v*), which facilitated the single-crystal X-ray diffraction experiment with Cu Kα radiation (Fig. 4). Consequently, the absolute configuration of compound **1** was unambiguously determined as 2*R*,4*R*,6*S*,7*S*,10*S*,1′*R*,5′*R*,6′*S*,7′*S*,10′*S*,11′*R*.

Artematrolide B (**2**) was isolated as white powders with a molecular formula of $C_{30}H_{38}O_6$ from the (+)-HRESIMS ion at *m*/*z* 517.2561 $[M+Na]^+$ (Calcd. for 517.2561), indicating 12 degrees of unsaturation. The ^{1}H and ^{13}C NMR data of **2** (Tables 1 and 4) highly resembled those of **1**, and the main difference was that the terminal olefinic carbon (δ_H 6.18 and 5.46, δ_C 139.9 and 119.4) in **1** was replaced with an ethylidene (δ_H 2.24 and 1.22, δ_C 42.2 and 12.8) in **2**. Taking its molecular weight (two Da higher than **1**) into consideration, compound **2** was reasonably deduced as the 11,13-dihydro derivative of **1**. The above deduction was confirmed by the ^{1}H−^{1}H COSY correlations of H_3-13/H-11/H-7, and HMBC correlations from H_3-13 (δ_H 1.22, overlapped) to C-7 (δ_C 50.2) and C-12 (δ_C 178.7), and from H-11 (δ_H 2.24, m) to C-6 (δ_C 80.3) and C-8 (δ_C 25.3). In the ROESY spectrum (Fig. 3), the cross peaks of H-7/H-11 and H-6/H_3-13 verified the β-orientation of the methyl at C-11. The absolute configuration of **2** was confirmed by means of ECD calculation. The calculated ECD spectrum matched well with the experimental one as shown in Fig. 5, confirming the absolute configuration as 2*R*,4*R*,6*S*,7*S*,10*S*,11*R*,1′*R*,5′*R*,6′*S*,7′*S*,10′*S*,11′*R*.

Artematrolide C (**5**) was assigned to a molecular formula of $C_{30}H_{36}O_6$ by the (+)-HRESIMS ion at *m*/*z* 493.2577 $[M+H]^+$ (Calcd. for 493.2585). Detailed interpretation of its ^{1}H and ^{13}C NMR data (Tables 1 and 4) proposed that compound **5** maintained the similar units A and B with compound **1**, and the differences in their NMR data of the cyclopentene moiety (unit A) indicated a different connecting model of two parts. In the HMBC spectrum (Fig. 2), the correlations from H-2 to C-7′, C-11′, and C-12′, and from H_2-13′ to C-1, C-4, C-5, and C-6 supported the connections of C-2–C-11′ and C-5–C-13′, instead of C-2–C-11′ and C-4–C-13′ in compound **1**. From a biosynthetic point of view, compound **5** was connected *via* a [4 + 2] Diels−Alder cycloaddition of arglabin as the dienophile[19] and the conjugated $\Delta^{2,4(5)}$-cyclopentadiene unit as the diene. In the ROESY spectrum (Fig. 3), the correlations of H-7/H-1 and H-6/H_3-14 manifested the α-orientation of H-1, and β-orientation of H-6 and CH_3-14. Similarly, H-5′ and H-6′/H-2 were respectively assigned as α- and β-orientated by the ROESY correlations of H-5′/H-7′ and H-6′/H-8′b/H-2. The α-orientation of CH_2-13′ was defined by the ROESY correlation of H-7′/H-13′a, which was consistent with that in compound **1**. Its absolute configuration was confirmed as 1*R*,2*S*,5*R*,6*S*,7*S*,10*R*,1′*R*,5′*R*,6′*S*,7′*S*,10′*S*,11′*R* by comparing the experimental ECD spectrum with the calculated one (Fig. 5).

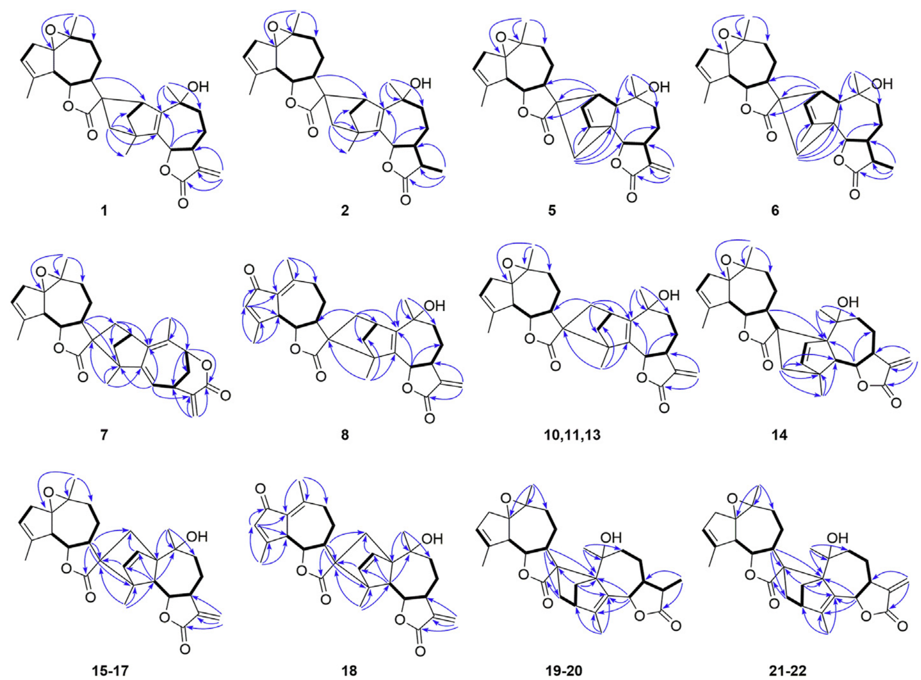

Figure 2 Selected 2D NMR correlations of compounds **1**, **2**, **5**−**8**, **10**, **11**, and **13**−**22**.

Artematrolide D (**6**) was deduced as the 11,13-dihydro derivative of compound **5** from its chemical composition with two additional hydrogens than compound **5**, and their highly similar NMR data (Tables 1 and 4) except for positions at C-11 and C-13. Compared with compound **5**, compound **6** showed the presence of a methine (δ_C 39.6) and a methyl (δ_C 9.3) but with the absence of a terminal olefinic group. This methyl group at C-11 was clearly assigned as β-orientated based on the $^1H-^1H$ COSY correlation of H-11/H-7, HMBC correlations (Fig. 2) from H_3-13 to C-7 and C-12, and ROESY correlation of H-6/H_3-13 (Fig. 3). Its absolute stereochemistry was assigned to be 1*R*,2*S*,5*R*,6*S*,7*S*,10*R*,11*R*,1′*R*,5′*R*,6′*S*,7′*S*,10′*S*,11′*R* by the high agreement between the experimental and calculated ECD spectra (Fig. 5).

Artematrolide E (**7**) had a molecular formula of $C_{30}H_{34}O_5$ deduced by the (+)-HRESIMS ion at *m*/*z* 475.2473 $[M+H]^+$ (Calcd. for 475.2479), revealing 14 hydrogen deficiency indices. The ^1H NMR data of **7** (Table 1) displayed signals of four singlet methyl groups at δ_H 1.14 (3H, s), 1.31 (3H, s), 1.93 (3H, s), and 2.03 (3H, s), an exocyclomethylene at δ_H 6.38 (1H, br.s) and 5.54 (1H, br.s), two oxygenated methines at δ_H 4.94 (1H, dd, $J=5.4$, 1.8 Hz) and 3.85 (1H, dd, $J=10.5$, 10.2 Hz), and two olefinic protons at δ_H 5.75 (1H, d, $J=8.4$ Hz) and 5.56 (1H, m). The ^{13}C NMR (DEPT) spectrum (Table 4) revealed 30 carbon resonances attributable to two ester carbonyls (δ_C 181.0, 165.6), terminal olefinic carbons (δ_C 136.1 and 129.4), trisubstituted olefinic carbons (δ_C 143.7, 125.6, 141.0, and 124.8), tetrasubstituted olefinic carbons (δ_C 142.7 and 129.2), four methyls, six sp^3 methylenes, six sp^3 methines (two oxygenated), and four sp^3 quaternary carbons. With the characteristic signals of two sets of lactone groups at δ_C 165.6 (C-12) and 181.0 (C-12′), it was suggested that compound **7** should be a dimeric sesquiterpene lactone.

By interpretation of the 2D NMR data ($^1H-^1H$ COSY and HMBC, Fig. 2) of compound **7**, four spin-coupling systems of H-6/H-7/H_2-8/H-9 and H-2/H_2-3 in unit A, and H-6′/H-7′/H_2-8′/H_2-9′ and H_2-2′/H-3′ in unit B were readily furnished by the $^1H-^1H$ COSY correlations. The HMBC correlations from H_2-13 to C-7, C-11, and C-12; from H_3-14 to C-1, C-9, and C-10; from H_3-15 to C-3, C-4, and C-5; from H-7 to C-5, C-9, C-12, and C-13; from H-9 to C-1, C-7, C-12, and CH_3-14 in unit A; and from H_3-14′ to C-1′, C-9′, and C-10′, from H_3-15′ to C-3′, C-4′, and C-5′, from H-7′ to C-5′, C-6′, C-8′, and C-9′, and from H-13′ to C-12′ in unit B were observed. Therefore, unit A was deduced as a six-membered lactone guaianolide moiety, and the unit B was determined to be similar to arglabin[19]. Moreover, the HMBC correlations of H_2-13′/C-1, C-2, and C-3, of H-3/C-11′ and C-13′, and of H_3-15/C-11′ indicated that units A and B were connected *via* two C−C single bonds between C-2−C-13′ and C-4−C-11′. Consequently, the planar structure of compound **7** was proposed as illustrated in Fig. 1.

The relative configuration of compound **7** was partially established by analysis of the ROESY data (Fig. 3). With the fact that C-7 of guaiane-type sesquiterpenoids always maintained the *S* configuration[37,44,45], the ROESY correlations of H-7/H-9, H-9/H_3-14, H_3-15/H-6, H_3-15/H-7′ and H-7/H-3b indicated that H-7, H-9, CH_3-15, and CH_2-3 were α-orientated, and the ROESY correlations of H-7′/H-5′/H-8′a assigned H-5′, H-8′a to be in α-orientation, while the ROESY correlations of H-6′/H-8′b/H-13′ deduced H-6′ and CH_2-13′ to be in β-configuration. This assignment was in accordance with the biogenetic origin of dimeric sesquiterpenes isolated from this genus. The absolute configuration of compound **7** was determined to be 2*S*,4*S*,7*R*,9*S*,1′*R*,5′*R*,6′*S*,7′*S*,10′*S*,11′*R* by comparison of its experimental ECD spectrum with the calculated one (Fig. 5).

Artematrolide F (**8**) was proposed to have a molecular formula of $C_{30}H_{34}O_6$ according to the (+)-HRESIMS ion at *m*/*z* 491.2413 $[M+H]^+$ (Calcd. for 491.2428). The ^1H NMR spectrum (Table 1) showed the signals of four methyl groups at δ_H 1.42, 1.50, 2.33, and 2.42 (each 3H, s), an exocyclomethylene at δ_H 6.11 (1H, d, $J=3.6$ Hz) and 5.57 (1H, overlapped), two oxygenated methines at δ_H 5.56 (1H, overlapped) and 3.65 (1H, dd, $J=10.0$, 9.6 Hz), and an olefinic proton at δ_H 6.16 (1H, s). The ^{13}C NMR spectrum

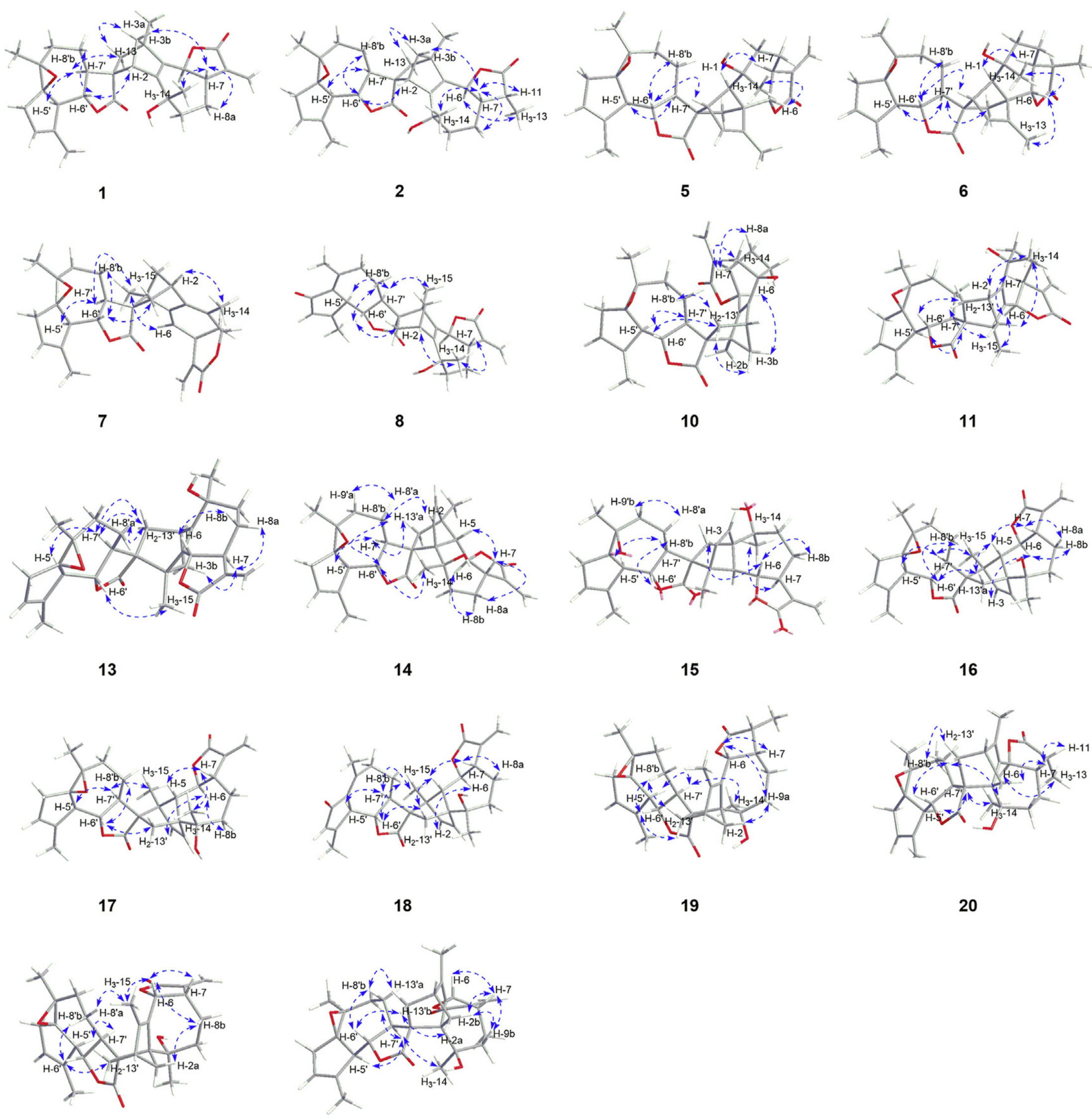

Figure 3 Key ROESY correlations of compounds **1**, **2**, **5**−**8**, **10**, **11**, and **13**−**22**.

(Table 4) of compound **8** exhibited 30 carbon resonances ascribe to four methyls, seven methylenes (including one exomethylene), seven methines, and twelve quaternary carbons. Further analyses of 1D and 2D NMR data gave rise to the construction of units A (identical with that in **1**) and B (dehydroleucodin[19]). The HMBC correlations (Fig. 2) of H_2-13′/C-1, C-2, and C-3; of H_3-15/C-11′ revealed that units A and B were connected *via* two C−C single bonds between C-2 and C-13′ and between C-4 and C-11′, identical to that in **7**. The ROESY correlations (Fig. 3) of H-3a with H-8′a, of H-8′a with H-7′ and the characteristic chemical shift of H-3a (δ_H 1.58) suggested the *endo* stereochemistry of compound **8** with the 2,4-linked form[47]. In addition, the cross peaks of H-7/H-3b, H-7/H_3-14, H_3-14/H-9b, H-7′/H-8′a, H-7′/H-5′, and H-7′/H_3-15 in the ROESY spectrum indicated that CH_2-3, CH_3-14, and H-5′ were α-orientated, while the cross peaks of H-6/H-9a, H-6′/H-8′b, H-6′/H_2-13′ revealed that H-6, H-6′, and CH_2-13′ were β-orientated. By means of ECD calculation (Fig. 5), its absolute configuration was established as 2*S*,4*S*,6*S*,7*S*,10*S*,5′*S*,6′*S*,7′*S*,11′*R*.

Artematrolide G (**10**) was obtained as colorless monoclinic crystals with a molecular formula of $C_{30}H_{36}O_6$ deduced by the (+)-HRESIMS ion at *m*/*z* 493.2538 $[M+H]^+$ (Calcd. for 493.2544). The ^1H and ^{13}C NMR data (Tables 2 and 4) of **10** showed high similarity with those of **1** with the main difference around the cyclopentene moiety, suggesting a different connecting model between two sesquiterpenoid parts. In the HMBC spectrum (Fig. 2), the correlations of H_2-13′/C-1 and C-3, of H-2/C-11′, of H-3/C-11′ and C-13′, and of H_3-15/C-11′ demonstrated the linkages of C-2−C-13′ and C-4−C-11′ in **10**. The coupling constant (10.4 Hz) of $J_{H\text{-}6/H\text{-}7}$ indicated the *trans*-axial orientation of H-6 and H-7, and H-6 was deduced as β-orientated. In the ROESY spectrum (Fig. 3), the correlations of H-7 with H_3-14 and H-6/H-3b verified the α-orientation of CH_3-14 and β-orientation of CH_2-3. Its structure was consolidated by the single-crystal X-ray diffraction analysis to be 2*R*,4*R*,6*S*,7*S*,10*S*,1′*R*,5′*R*,6′*S*,7′*S*,10′*S*,11′*R* (Fig. 4).

Compound **11** had the same molecular formula and similar ^1H and ^{13}C NMR data (Tables 2 and 4) with **10**, indicating the closely related structures. The same planar structure of **11** with **10** was determined by detailed interpretation of its $^1H-^1H$ COSY and HMBC experiments (Fig. 2). Compared with **10**, the

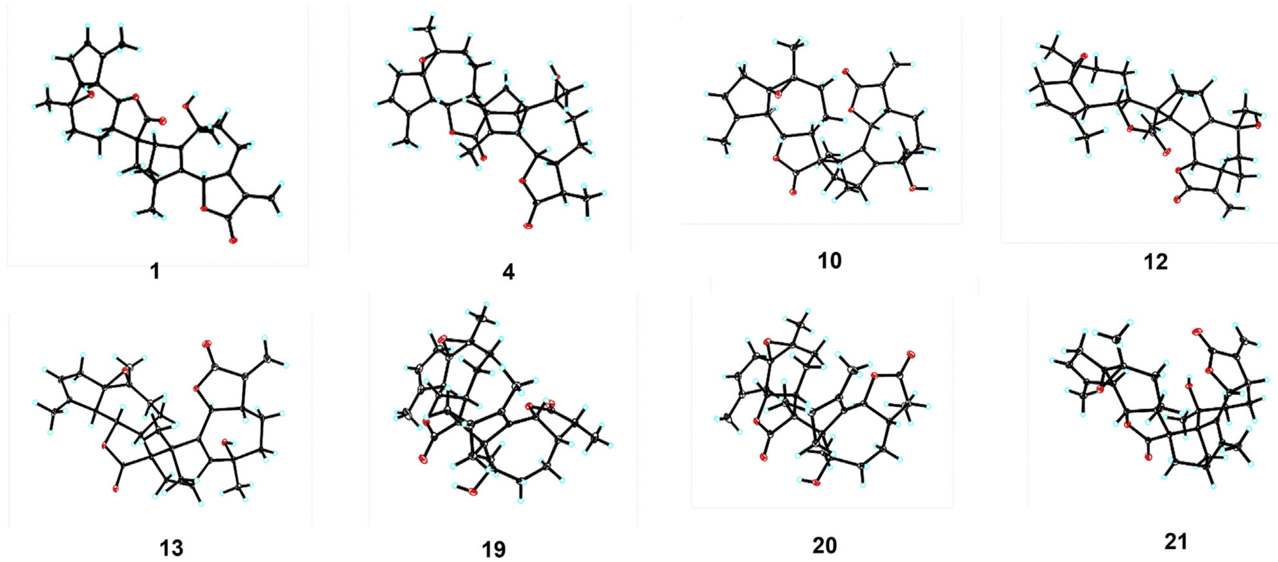

Figure 4 ORTEP drawings of compounds **1**, **4**, **10**, **12**, **13**, and **19**–**21**.

chemical shifts of C-3 in **11** was changed to δ_C 52.4 (*vs.* 56.8 in **10**), and C-8 and C-14 were de-shielded to δ_C 28.4 (*vs.* 21.7 in **10**) and 29.0 (*vs.* 25.2 in **10**), respectively, suggesting the varied stereochemistry. The coupling constant (6.6 Hz) of $J_{H\text{-}6/H\text{-}7}$ indicated the *cis*-axial orientation of H-6 and H-7, *i.e.*, H-6 was deduced as α-orientated. Furthermore, the cross peaks of H-6/H_3-15 and H_3-15/H-7′, H-7′/H-5′ indicated that H-5′ and CH_3-15 was α-configuration, while the correlations of H_3-14/H-2, H_3-14/H-3b, H-6′/H_2-13′, H-6′/H-8′b, and H-8′b/H-13′a in the ROESY spectrum revealed that CH_2-3, CH_3-14, and CH_2-13′ was β-orientated (Fig. 3). By comparing the experimental and calculated ECD spectrum (Fig. 5), its absolute configuration was assigned as 2*R*,4*R*,6*R*,7*S*,10*R*,1′*R*,5′*R*,6′*S*,7′*S*,10′*S*,11′*R*.

Compound **13** had a molecular formula of $C_{30}H_{36}O_6$ from the (+)-HRESIMS ion at *m/z* 493.2069 $[M+H]^+$ (Calcd. for 493.2068). The ^{13}C NMR data of **13** were very similar to those of **12**, and the main differences were observed at C-1, C-3, C-5, C-6, C-7′, C-12′, and C-13′ (Table 4 and Table S2). By detailed interpretation of its $^1H-^1H$ COSY and HMBC data (Fig. 2), the identical planar structure of **13** with **12** was constructed. In the ROESY spectrum (Fig. 3), the correlations of H-7/H-3b, H-7/H-8a, H-7′/H_2-13′, H-7′/H-8′a, H-8′a/H-13′b verified the α-orientation of CH_2-3 and CH_2-13′, while the ROESY correlation of H-6/H-8b together with the big coupling constant ($J_{H\text{-}6/H\text{-}7} = 9.6$ Hz) assigned H-6 as β-orientated. The structure of **13** was confirmed though a single crystal X-ray diffraction experiment with Cu Kα radiation [Flack parameter of 0.03(6)], and the absolute configuration was confirmed as 2*S*,4*S*,6*S*,7*S*,10*S*,1′*R*,5′*R*,6′*S*,7′*S*,10′*S*,11′*S* (Fig. 4). Consequently, the structure of **13** was established and named as artematrolide I.

Artematrolide J (**14**) was assigned a molecular formula of $C_{30}H_{36}O_6$ from the (+)-HRESIMS ion at *m/z* 493.2594 $[M+H]^+$ (Calcd. for 493.2585). By detailed interpretation of the 1D and 2D NMR data (Tables 2 and 5), compound **14** was proposed as a guaianolide dimer similar with compound **13**. Differently, the two units of compound **14** were deduced to be linked *via* C-1–C-11′ and C-4–C-13′ based on the HMBC correlations of H_2-13′/C-3, C-4, C-5, and C-15, of H-2/C-11′, of H-5/C-11′ and C-13′, and of H_3-15/C-13′ (Fig. 2). In the ROESY spectrum, cross signals detected for H-7/H-5, H-7/H-8a, H-5/H-2, H-5/H-3, H-7′/H-5′, and H-7′/H-8′a suggested the α-orientation of H-5, H-5′, and the ethenylene (C-2–C-3), the correlation of H-7′/H-13′, H-8′a/H-13′a revealed the same orientation H-7′ and CH_2-13′, while the cross signals of H-6/H-8b, H-8b/H_3-14, H-6/H_3-14, and H-6′/H-8′b indicated the β-orientation of H-6, H-6′, and CH_3-14 (Fig. 3). By virtue of ECD calculation, the absolute configuration of compound **14** was determined as 1*S*,4*S*,5*S*,6*S*,7*S*,10*R*,1′*R*,5′*R*,6′*S*,7′*S*,10′*S*,11′*R* (Fig. 5).

Artematrolide K (**15**) was assigned the same molecular formula of $C_{30}H_{36}O_6$ as that of compound **14** by the (+)-HRESIMS ion at *m/z* 493.2550 $[M+H]^+$ (Calcd. for 493.2561). The ^1H and ^{13}C NMR data (Tables 2 and 5) of compound **15** was highly resembled artemyriantholide D[19], indicating the closely related structures. By further interpretation of its $^1H-^1H$ COSY and HMBC spectra (Fig. 2), compound **15** was proposed the same planar structure with artemyriantholide D. The differences in their NMR data should be ascribed to the changed stereochemistry in structures. Compared with artemyriantholide D, the chemical shifts of C-1, C-9, and C-14 were shifted from δ_C 62.8, 34.7, and 29.8 in artemyriantholide D to 63.2, 36.3, and 21.8 in compound **15**. In the ROESY spectrum (Fig. 3), the correlations of H-5 and H-7 with H_3-14 suggested the α-orientation of CH_3-14, and compound **15** was deduced as the 10-epimer of artemyriantholide D. The absolute configuration of compound **15** was elucidated as 1*R*,4*R*,5*S*,6*S*,7*S*,10*S*,1′*R*,5′*R*,6′*S*,7′*S*,10′*S*,11′*S* *via* quantum chemical calculation (Fig. 5).

Artematrolide L (**16**) maintaining a molecular formula of $C_{30}H_{36}O_6$ was deduced from the (+)-HRESIMS ion at *m/z* 493.2583 $[M+H]^+$ (Calcd. for 493.2585). Detailed analyses of its ^1H and ^{13}C NMR data (Tables 2 and 5) suggested that compound **16** was an isomer of artemyriantholide D, and the main differences were located at C-1 (δ_C 63.8), C-2 (δ_C 133.2), C-3 (δ_C 142.0), and C-4 (δ_C 57.1) in contrast to δ_C 62.8, 135.8, 138.3, and 61.2 in artemyriantholide D. In the ROESY spectrum, the cross peaks of H-7/H-5, H-7/H-8a, H-7′/H-5′, H-7′/H-8′a, and H-7′/H_3-15 proposed the α-orientation of H-5 and H-5′, while the cross peaks of H-6/H-2, H-6/H-3, H-6/H-8b, H-6/H_3-14, H-6′/H-8′b, and H-6′/H_2-13′ manifested the β-orientation of H-6, H-6′, CH_3-14, CH_2-13′, and the ethenylene (C-2–C-3, Fig. 3). Thus, compound **16** was determined as the 11′-epimer of artemyriantholide D. The

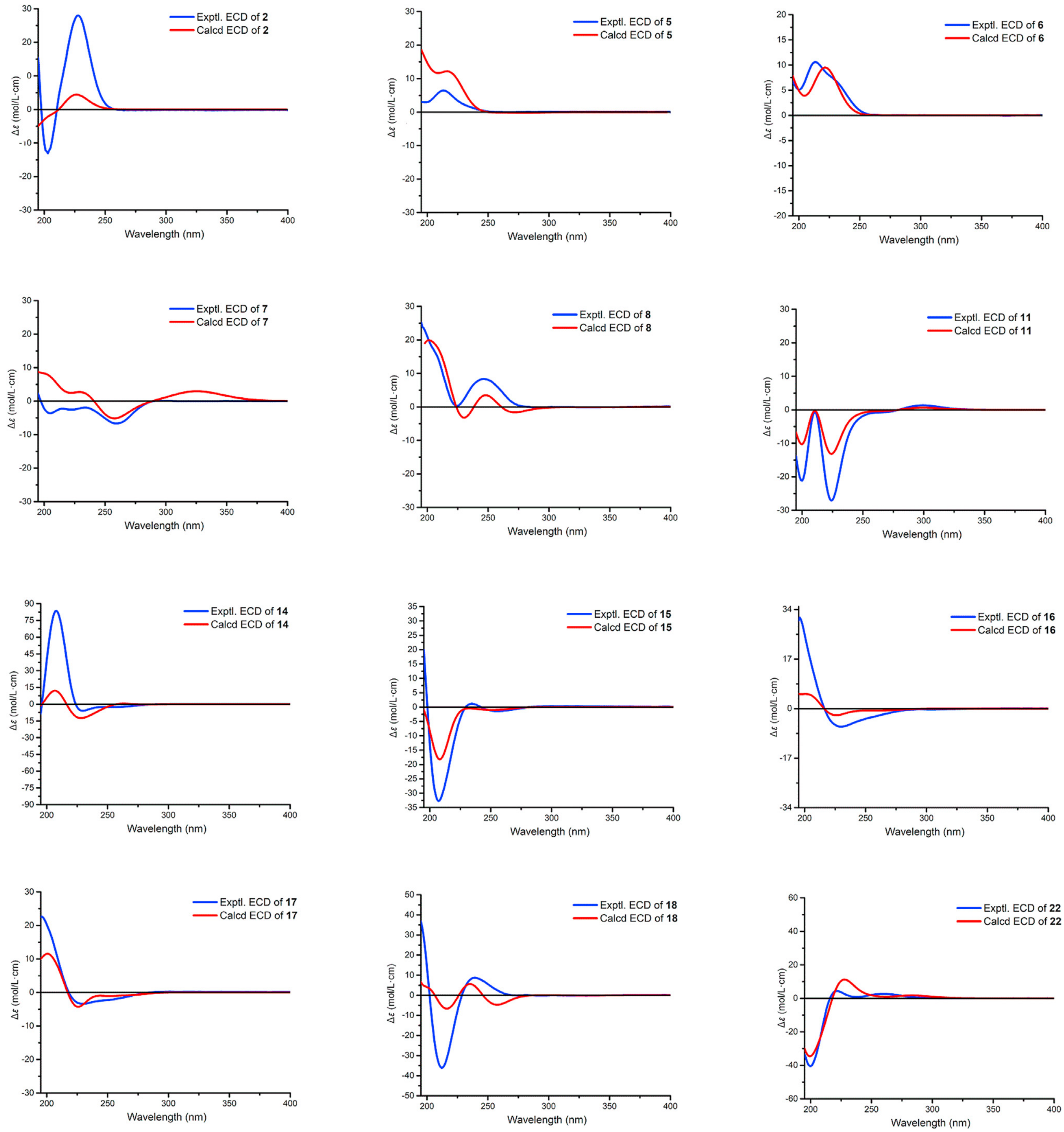

Figure 5 Experimental and calculated ECD spectra of compounds **2**, **5**–**8**, **11**, **14**–**18**, and **22**.

calculated ECD curve for compound **16** well matched that of the experimental one (Fig. 5), which allowed the assignment of its absolute configuration as 1*R*,4*R*,5*S*,6*S*,7*S*,10*R*,1′*R*,5′*R*,6′*S*,7′*S*,10′*S*,11′*R*.

Artematrolide M (**17**) had the same molecular formula of $C_{30}H_{36}O_6$ with compound **16** by the (+)-HRESIMS ion at *m*/*z* 493.2551 $[M+H]^+$ (Calcd. for 493.2561). Analyses of the 1D NMR data (Tables 3 and 5) suggested that compound **17** had the same planar structure with compound **16**. By comparison with **16**, the chemical shift of C-14 was significantly shielded from δ_C 30.0 in **16** to 23.6 in **17**, suggesting the varied stereochemistry at C-14. In the ROESY spectrum (Fig. 3), the correlation of H-7/H_3-14, H-7/H-5, H-7/H-8a was readily detected, supporting the *α*-configuration of H-7, H-5 and CH_3-14, while the cross peaks of H-6/H-8b, H-6/H-3, H-6/H-2 together with the large coupling constant ($J_{H\text{-}6/H\text{-}7}$ = 9.6 Hz) indicated the *β*-orientation of H-6 and the ethenylene (C-2–C-3), by which compound **17** was determined as the 10-epimer of compound **16**. The relative configuration of unit B was confirmed by the ROESY experiment, which was the same as that of compound **16**. By means of ECD calculation (Fig. 5), the absolute configuration of **17** was assigned as 1*R*,4*R*,5*S*,6*S*,7*S*,10*S*,1′*R*,5′*R*,6′*S*,7′*S*,10′*S*,11′*R*.

Table 2 ^{1}H NMR spectroscopic data for compounds **10**, **11**, and **13**−**16** (δ in ppm, J in Hz).

No. position	**10**[a,d]	**11**[a,c]	**13**[b,d]	**14**[a,c]	**15**[b,d]	**16**[a,c]
2	3.19 m	3.05 (overlapped)	2.90 m	5.86 d (5.4)	6.41 d (5.6)	5.85 d (5.7)
3	2.75 m	2.58 dd (9.0, 1.2)	2.36 dd (8.3, 1.6)	6.00 d (5.4)	5.86 d (5.6)	6.34 d (5.7)
	1.43 m	1.35 m	1.25 dd (8.3, 2.4)			
5				2.99 d (10.2)	2.96 d (10.0)	2.31 d (9.9)
6	4.87 d (10.4)	4.70 d (6.6)	5.29 d (9.6)	4.06 dd (10.2, 9.6)	4.17 dd (10.0, 9.6)	4.18 dd (9.9, 9.6)
7	2.98 m	3.05 (overlapped)	2.91 m	3.43 m	2.87 m	3.26 m
8	2.19 m	1.87 m	2.24 m	2.27 m	2.26 m	2.23 m
	1.71 m	1.74 m	1.87 (overlapped)	1.34 m	1.60 m	1.48 m
9	2.02 m	1.92 m	1.91 m	1.90 m	2.05 m	1.88 m
	1.90 m	1.74 m	1.87 (overlapped)	1.84 (overlapped)	1.81 m	1.84 m
13	6.22 d (3.2)	6.29 d (1.2)	6.14 d (3.6)	6.08 d (3.3)	6.05 d (3.4)	6.10 d (3.6)
	5.51 d (3.2)	5.70 d (1.2)	5.60 d (3.6)	5.36 d (3.3)	5.50 d (3.4)	5.37 d (3.6)
14	1.37 s	1.43 s	1.44 s	1.45 s	1.44 s	1.30 s
15	1.41 s	1.34 s	1.47 s	1.44 s	1.49 s	1.35 s
2′	2.73 m	2.73 br d	2.80 m	2.72 br d	2.80 m	2.77 dd (17.9, 3.3)
	2.09 m	2.12 m	2.12 m	2.12 br d	2.13 (overlapped)	2.15 (overlapped)
3′	5.55 m	5.56 m	5.61 m	5.57 br s	5.61 m	5.55 m
5′	2.93 d (10.2)	2.82 d (10.2)	2.81 m	2.83 d (10.2)	2.78 m	2.82 d (10.2)
6′	3.88 dd (10.4, 10.2)	3.90 dd (10.2, 10.2)	4.30 dd (10.4, 10.4)	3.99 dd (10.2, 10.2)	4.32 dd (10.4, 10.4)	4.06 dd (10.2, 9.0)
7′	1.90 m	1.58 m	1.83 m	2.36 m	1.82 m	1.94 m
8′	1.31 m	1.43 m	1.71 m	1.63 m	1.69 m	1.72 m
	1.16 m	1.29 m	1.46 m	1.33 m	1.29 m	1.69 m
9′	1.81 m	2.10 m	2.18 m	2.02 m	2.13 (overlapped)	2.14 (overlapped)
	1.74 m	1.81 m	1.88 m	1.83 m	1.84 m	2.00 m
13′	1.98 m	1.98 dd (12.6, 4.2)	2.49 dd (12.4, 4.4)	1.84 (overlapped)	2.51 d (12.3)	2.40 d (11.7)
	1.70 m	1.77 m	1.45 m	1.75 d (12.0)	1.40 d (12.3)	1.40 d (11.7)
14′	1.25 s	1.33 s	1.33 s	1.29 s	1.32 s	1.34 s
15′	1.96 s	1.95 s	1.97 s	1.95 s	1.97 s	1.92 s

[a]Recorded in $CDCl_3$. [b]Recorded in CD_3OD. [c]Recorded at 600 MHz. [d]Recorded at 400 MHz.

Artematrolide N (**18**) was obtained as a white amorphous powder with a molecular formula of $C_{30}H_{34}O_6$ by the (+)-HRESIMS ion at m/z 491.2435 $[M+H]^+$ (Calcd. for 491.2428). By comparison with compound **16**, one methylene (C-2′) and two epoxidized carbons (C-1′ and C-10′) in compound **16** were replaced by a carbonyl (δ_C 195.9) and two non-protonated sp^2 carbons (δ_C 131.8 and 152.0) in compound **18**. Thus, a 1,4-dien-3-one partial structure was identical with that in compound **8**, which was supported by the consistent correlations from H-3′ to C-1′, from H_3-15′ to C-3′, from H-5′ to C-2′, C-3′, and C-10′, and from H_3-14′ to C-1′ in the HMBC spectrum (Fig. 2). The relative configuration of compound **18** was determined based on the ROESY experiment, the cross peaks of H-7/H-5, H-7/H-8a, H-7′/H-5′, H-7′/H-8′a in the ROESY spectrum suggested the α-orientation of H-5 and H-5′, while the cross peaks of H-6/H-2, H-6/H-3, H-6/H-8b, H-2/H_3-14, H-6′/H-8′b indicated the β-orientation of H-6, H-6′, CH_3-14, and the ethenylene (C-2−C-3, Fig. 3). Moreover, the β-orientation of CH_2-13′ was confirmed by the correlation between H-6′ and H_2-13′ in the ROESY spectrum. By comparing the experimental and calculated ECD spectra (Fig. 5), the absolute configuration of compound **18** was determined as 1*R*,4*R*,5*S*,6*S*,7*S*,10*R*,5′*S*,6′*S*,7′*S*,11′*R*.

Artematrolide O (**19**) had a molecular formula of $C_{30}H_{38}O_6$ from the (+)-HRESIMS ion at m/z 517.2558 $[M+Na]^+$ (Calcd. for 517.2561), indicating 12 degrees of unsaturation. Comprehensive analyses of its ^{1}H and ^{13}C NMR spectroscopic data (Tables 3 and 5) indicated close resemblances to artemyriantholide C[19]. Its planar structure and partial relative configuration were reported, but its absolute configuration has not been determined. In the ROESY spectrum, the cross peaks of H-7/H-6, H-7/H-9a, H-6/H-9a, H-7/H-11, and H-6/H-11, together with the small coupling constant ($J_{H\text{-}6/H\text{-}7}$ = 3.6 Hz) indicated that H-6 and H-11 were α-orientated, while correlation of H_3-14 with H-9b assigned the β-orientation of CH_3-14. Similarly, the correlation of H-7′ with H-5′ and the large coupling constant ($J_{H\text{-}6'/H\text{-}7'}$ = 10.2 Hz) assigned the α-orientation of H-5′ and H-7′, and β-orientation of H-6′. Owing to the lack of ROESY correlations, the relative configuration of the additional cyclohexene moiety could not be confirmed. A single-crystal X-ray diffraction for compound **19** was performed using the Cu Ka radiation [Flack parameter of 0.06 (4)] (Fig. 4). Therefore, the structure of compound **19** was established, and its absolute configuration was assigned to be 1*S*,3*R*,6*R*,7*S*,10*R*,11*R*,1′*R*,5′*R*,6′*S*,7′*S*,10′*S*,11′*R*.

Artematrolide P (**20**) possessed the same molecular formula with **19** by the (+)-HRESIMS ion at m/z 517.2556 $[M+Na]^+$ (Calcd. for 517.2561). Detailed analyses of the 1D and 2D NMR data (Tables 3 and 5) revealed that compound **20** possessed the same planar structure with compound **19**. In the ^{13}C NMR (DEPT) spectrum, the chemical shifts of C-6, C-7, and C-11 were shifted from δ_C 77.3, 45.2, and 43.5 in compound **19** to 82.4, 49.7, and 38.8 in compound **20**, respectively, suggesting the different configuration. In the ^{1}H NMR spectrum, H-6 was present at δ_H 4.42 with a large coupling constant ($J_{H\text{-}6/H\text{-}7}$ = 11.2 Hz), obviously different from **19** (δ_H 5.01, d, J = 3.6 Hz), indicating the β-orientation of H-6 in **20**. The ROESY spectrum supported this deduction by the correlations of H-7 with H-8a, H-6 with H-8b

Table 3 ^{1}H NMR spectroscopic data for compounds **17**−**22** (δ in ppm, J in Hz).

No.	**17**[a,b]	**18**[a,c]	**19**[a,b]	**20**[a,c]	**21**[a,c]	**22**[a,b]
2	6.23 d (5.4)	5.99 d (5.6)	2.43 dd (9.6, 1.4)	2.23 m	2.69 m	2.46 m
			1.77 dd (9.6, 3.2)	1.58 m	1.40 m	1.79 dd (9.6, 3.2)
3	6.34 d (5.4)	5.80 d (5.6)	2.66 m	2.54 m	2.67 m	2.68 m
5	2.05 m	3.13 d (10.0)				
6	4.26 dd (10.2, 9.6)	4.04 dd (10.0, 9.6)	5.01 d (3.6)	4.42 d (11.2)	5.50 br d	5.06 d (4.2)
7	2.70 m	3.35 m	2.26 m	2.23 m	3.37 m	2.85 m
8	2.17 m	2.29 m	1.71 m	1.70 m	1.86 m	1.86 (overlapped)
	1.62 m	1.45 m	1.33 m	1.49 m	1.81 m	1.62 m
9	2.08 m	1.90 m	1.91 m	1.82 m	1.88 (overlapped)	2.03 (overlapped)
	1.79 m	1.82 m	1.59 m	1.65 m	1.60 m	1.55 m
11			2.80 m	2.67 m		
13	6.14 d (3.3)	6.09 d (3.4)	1.20 d (7.1)	1.16 d (8.0)	6.19 d (2.6)	6.08 br s
	5.41 d (3.3)	5.36 d (3.4)			5.46 d (2.6)	5.54 br s
14	1.38 s	1.32 s	1.38 s	1.39 s	1.31 s	1.42 s
15	1.36 s	1.45 s	1.84 s	1.88 s	1.86 s	1.83 s
2′	2.77 dd (17.9, 2.2)		2.74 dd (17.7, 3.7)	2.69 m	2.72 m	2.75 m
	2.16 m		2.11 dd (17.7, 2.4)	2.08 m	2.10 m	2.03 m
3′	5.56 m	6.18 s	5.57 m	5.54 m	5.52 m	5.58 m
5′	2.82 m	3.25 d (10.0)	2.91 m	2.82 d (10.4)	2.91 d (10.4)	2.92 d (10.2)
6′	4.06 dd (10.2, 9.6)	3.94 dd (10.4, 10.0)	3.99 dd (10.2, 10.2)	3.96 dd (10.4, 10.0)	3.82 dd (10.4, 10.0)	4.00 dd (10.2, 10.2)
7′	1.93 (overlapped)	2.34 m	2.24 m	2.04 m	2.84 m	2.25 m
8′	1.69 m	1.89 m	1.16 m	1.42 m	1.17 m	1.18 m
	1.66 m	1.17 m	1.10 m	1.23 m	1.09 m	1.15 m
9′	2.14 m	2.30 m	2.28 m	2.13 m	2.46 m	2.35 m
	2.02 m	2.22 m	1.93 m	1.66 m	1.99 m	1.98 m
13′	2.25 d (12.1)	2.69 d (11.8)	1.89 m	1.77 m	1.88 (overlapped)	1.91 dd (12.0, 3.8)
	1.58 d (12.1)	1.31 m	1.82 dd (12.0, 3.2)	1.72 m	1.59 m	1.84 m
14′	1.35 s	2.41 s	1.30 s	1.26 s	1.32 s	1.31 s
15′	1.92 s	2.31 s	1.96 s	1.91 s	1.93 s	1.96 s

[a]Recorded in $CDCl_3$. [b]Recorded at 600 MHz. [c]Recorded at 400 MHz.

(Fig. 3). A single-crystal X-ray diffraction analysis of compound **20** by utilizing Cu Kα radiation established its absolute configuration as 1*S*,3*R*,6*S*,7*S*,10*R*,11*R*,1′*R*,5′*R*,6′*S*,7′*S*,10′*S*,11′*R* (Fig. 4).

Artematrolide Q (**21**) was assigned to a molecular formula of $C_{30}H_{36}O_6$ by the (+)-HRESIMS ion at *m/z* 493.2575 $[M+H]^+$ (Calcd. for 493.2585). By detailed inspection of its 1D and 2D NMR data (Tables 3 and 5), the same planar structure with artemyriantholide B was determined[19]. By comparison with artemyriantholide B, the chemical shifts of C-4, C-6, and C-7 were shifted from δ_C 142.6, 82.9, and 50.9 in artemyriantholide B to δ_C 152.0, 75.1, and 39.6 in compound **21**, respectively. In the ROESY spectrum (Fig. 3), the correlation of H-6/H-7 was readily observed, indicating the α-orientation of H-6. The absolute configuration of **21** was elucidated as 1*S*,3*R*,6*R*,7*S*,10*S*,1′*R*,5′*R*,6′*S*,7′*S*,10′*S*,11′*R* *via* the single-crystal X-ray diffraction experiment (Fig. 4).

Artematrolide R (**22**) had a molecular formula of $C_{30}H_{36}O_6$ as deduced from the (+)-HRESIMS ion at *m/z* 515.2405 $[M+Na]^+$ (Calcd. for 515.2404). The ^{1}H and ^{13}C NMR data (Tables 3 and 5) of compound **22** were very similar to those of compound **19** with the main differences at C-8, C-11, C-12, and C-13. The terminal olefinic carbons were easily recognized in compound **22** from the characteristic protons and carbons (δ_H 6.08 and 5.54, δ_C 142.3 and 119.2), instead of a methine and a methyl in compound **19**. Taking its molecular formula that was two hydrogens less than compound **19** into consideration, compound **22** was deduced as the 11,13-dehydro derivative of compound **19**, which was confirmed by the correlations from H_2-13 to C-7 and C-12 in the HMBC experiment (Fig. 2). The correlations of H-7/H-6, H-7/H-8a, H-7/H-9a, and H-9a/H-2b in the ROESY spectrum, and the small coupling constant ($J_{H\text{-}6/H\text{-}7}$ = 4.2 Hz) indicated that H-6 and CH_2-3 were α-orientated, while the cross signal of H_3-14 with H-8b assigned the β-orientation of CH_3-14. The correlation of H-7′ with H-5′ and the large coupling constant ($J_{H\text{-}6'/H\text{-}7'}$ = 10.2 Hz) characterized the α-configuration of H-5′ and H-7′, and β-orientation of H-6′. Similarly, the correlation between H-6′ and H_2-13′ manifested CH_2-13′ as β-orientated. Further analysis of its ROESY spectrum (Fig. 3) suggested the same relative configuration of compound **22** with compound **19**. The absolute configuration of compound **22** was determined by comparing the calculated ECD spectrum with the experimental one (Fig. 5). Hence, the structure of **22** was established and named as artematrolide R.

Compounds **3**, **4**, **9**, **12**, and **23** were identified as lavandiolides A, B, J, H, and C by comparison of their NMR data with the data in Ye's paper[42], and the structures of lavandiolides B, H were confirmed by single-crystal X-ray diffraction in our report.

The EtOH extract and EtOAc fraction of *A. atrovirens* were tested for their inhibitory activity on HepG2 cells with inhibitory ratios of 98.9% and 95.9% at 100.0 μg/mL (Fig. 6). The EtOAc fraction was separated into three subfractions (Fr. 1−Fr. 3), of which Fr. 2 showed obvious cytotoxicity with the inhibitory ratio of 98.6%, more potent than two other subfractions [Fr. 1 (55.9%) and Fr. 3 (41.5%)] at 100.0 μg/mL.

The obtained compounds (**1**−**23**) from Fr. 2 were evaluated on three human hepatoma cell lines (HepG2, SMMC-7721, and Huh7), and the results were shown in Table 6. For HepG2 cells, five compounds (**1**, **3**, **5**, **12**, and **13**) exhibited cytotoxicity with

Table 4 ^{13}C NMR spectroscopic data for compounds **1**, **2**, **5−8**, **10**, **11**, and **13** (δ in ppm).

No.	**1**[a,c]	**2**[a,c]	**5**[b,d]	**6**[b,d]	**7**[a,c]	**8**[b,d]	**10**[a,d]	**11**[a,c]	**13**[b,d]
1	148.6	147.8	69.6	69.4	142.7	153.1	158.4	157.9	154.9
2	48.7	48.6	46.0	46.0	41.2	42.5	41.4	42.9	42.0
3	55.1	55.0	125.1	124.8	42.3	53.1	56.8	52.4	55.8
4	54.6	54.4	144.5	144.7	57.2	59.5	61.2	60.4	61.0
5	144.9	145.3	57.3	57.5	143.7	143.0	139.1	132.9	140.4
6	80.2	80.3	83.6	83.0	125.6	83.7	78.3	77.0	82.5
7	46.6	50.2	42.0	40.5	35.4	46.3	45.4	45.0	46.9
8	23.7	25.3	25.5	23.2	27.2	22.8	21.7	28.4	23.8
9	37.9	38.4	45.4	45.6	81.0	37.4	39.8	39.7	37.7
10	71.4	70.8	72.5	72.4	129.2	71.9	73.0	73.7	71.4
11	139.9	42.2	139.8	39.6	136.1	140.6	139.2	141.0	140.0
12	170.2	178.7	170.9	181.1	165.6	170.7	169.4	169.7	170.4
13	119.4	12.8	119.4	9.3	129.4	118.3	119.9	122.7	118.7
14	28.6	28.8	25.8	25.8	21.1	25.5	25.2	29.0	26.5
15	20.4	20.3	11.5	11.5	13.6	16.1	13.5	12.7	17.4
1′	72.1	72.0	72.2	72.1	73.0	131.8	72.8	72.8	72.4
2′	39.3	39.1	38.5	38.5	39.8	196.8	39.4	39.7	38.8
3′	125.2	125.1	124.9	124.8	124.8	134.6	124.6	125.0	124.6
4′	140.9	140.8	140.6	140.6	141.0	172.9	140.9	141.1	140.6
5′	52.0	51.9	51.6	51.6	54.1	52.0	53.2	53.8	53.3
6′	81.4	81.3	81.2	81.2	81.3	81.7	81.0	81.1	81.7
7′	55.7	55.7	54.6	54.6	50.2	53.8	49.4	50.3	56.4
8′	21.1	21.0	20.8	20.8	22.7	23.9	22.7	23.0	19.5
9′	33.3	33.2	32.6	32.6	34.5	36.1	33.0	34.3	33.7
10′	62.1	61.9	62.2	62.2	63.0	153.4	62.6	62.6	62.6
11′	55.9	55.5	53.8	53.6	52.8	56.4	54.4	54.7	56.8
12′	183.6	183.6	179.8	179.8	181.0	179.6	180.8	180.9	182.5
13′	42.8	42.6	34.5	35.0	34.7	34.3	35.1	34.6	41.0
14′	22.7	22.6	21.4	21.3	22.8	19.8	22.5	22.8	21.3
15′	18.8	18.6	17.5	17.5	18.6	18.9	18.6	18.7	17.4

[a]Recorded in $CDCl_3$. [b]Recorded in CD_3OD. [c]Recorded at 150 MHz. [d]Recorded at 100 MHz.

IC_{50} values of 4.4, 5.5, 3.3, 3.8, and 5.3 μmol/L, which were superior to the positive control, sorafenib (IC_{50} 7.7 μmol/L); six compounds (**7**, **14−16**, **19**, and **22**) exhibited cytotoxic activity with IC_{50} values of 6.0, 7.6, 6.7, 8.8, 7.1, and 6.4 μmol/L, which were comparable to sorafenib.

For SMMC-7721 cells, three compounds (**12**, **14**, and **15**) indicated cytotoxicity with IC_{50} values of 4.6, 6.6, and 6.0 μmol/L, which were more potent than sorafenib (IC_{50} 9.9 μmol/L); five compounds (**1**, **6**, **8**, **18**, and **21**) exhibited cytotoxicity with IC_{50} values of 9.6, 8.9, 8.9, 11.4, and 10.1 μmol/L, and were similar with sorafenib.

For Huh7 cells, seven compounds (**3**, **5**, **6**, **8**, **12**, **13**, and **15**) displayed cytotoxicity with IC_{50} values of 5.4, 5.7, 4.5, 5.9, 4.5, 4.0, and 5.6 μmol/L, which manifested those compounds were more potent than the positive control, sorafenib (IC_{50} 8.3 μmol/L); six compounds (**1**, **10**, **11**, **14**, **17**, and **20**) possessed cytotoxicity with IC_{50} values of 7.6, 8.2, 9.1, 6.9, 8.4, and 10.4 μmol/L, and were comparable to sorafenib. Compounds **7**, **19**, and **22** manifested cytotoxicity only to HepG2 cells with IC_{50} values of 6.0, 7.1, and 6.4 μmol/L. Compounds **6** and **8** showed inhibitory activity on both SMMC-7721 and Huh7 cells.

Interestingly, compounds **3**, **5**, and **13** showed inhibitory activity on both HepG2 and Huh7 cells, which were superior to sorafenib. Four compounds (**1**, **12**, **14**, and **15**) exhibited inhibitory activity on the three cell lines with IC_{50} values of 4.4, 3.8, 7.6, and 6.7 μmol/L (HepG2), 9.6, 4.6, 6.6, and 6.0 μmol/L (SMMC-7721), and 7.6, 4.5, 6.9, and 5.6 μmol/L (Huh7), respectively. Compound **12** showed the highest cytotoxicity against three human hepatoma cell lines, which were superior to sorafenib.

To understand the effects of compound **12** on hepatoma metastasis, the potential impact of compound **12** on HCC metastasis was investigated by using cell migration and invasion assays. The results indicated that compound **12** suppressed HepG2 cell migration and invasion in a dose-dependent manner. Comparing with the control cells, the migration ratio of HepG2 cells was reduced to 84.9%, 69.2% and 37.5% at 1.0, 2.0 and 4.0 μmol/L, respectively. The invasion rate was decreased to 85.6% (1.0 μmol/L), 64.6% (2.0 μmol/L) and 43.0% (4.0 μmol/L). Consistently, these results were indicative of a potential effect of compound **12** on HCC migration (Fig. 7).

To investigate the cytotoxic mechanism of compound **12**, the cell cycle progression and apoptosis effects on HepG2 cells were analyzed by flow cytometry. The composition of cells in various phases varied according to concentration when the cells were treated with different concentrations (0.0, 2.0, 4.0 and 8.0 μmol/L) of compound **12**, and the cell ratio in different stages varied following the alterations of concentration. After being treated with different concentrations of compound **12**, the percentage of cells in the G2/M phase increased from 13.3% to 16.6% (2.0 μmol/L), 19.3% (4.0 μmol/L) and 25.1% (8.0 μmol/L) independently by comparison to the control cells. These results demonstrated that compound **12** effectively induced a cell cycle arrest in G2/M phase (Fig. 8). Next, we investigated the expression of cell cycle regulators which control the G2/M transition. As shown in

Table 5 ^{13}C NMR spectroscopic data for compounds **14**–**22** (δ in ppm).

No.	**14**[a,c]	**15**[b,d]	**16**[a,c]	**17**[a,c]	**18**[a,d]	**19**[a,c]	**20**[a,d]	**21**[a,d]	**22**[a,c]
1	71.6	63.2	63.8	64.3	62.8	73.5	71.5	70.5	74.0
2	133.4	136.8	133.2	133.5	136.4	49.2	46.9	47.7	49.3
3	140.8	136.3	142.0	141.2	137.7	44.7	45.4	46.0	44.8
4	52.0	61.4	57.1	57.7	61.1	153.3	142.8	152.0	154.3
5	68.3	66.2	66.6	66.6	66.8	133.6	134.5	135.7	133.0
6	80.3	79.0	80.3	79.1	79.3	77.3	82.4	75.1	76.5
7	43.8	43.4	43.6	44.0	43.2	45.2	49.7	39.6	45.8
8	23.9	22.6	23.6	23.0	23.6	21.7	21.8	25.4	28.0
9	38.2	36.3	35.0	37.0	34.6	39.1	41.0	41.1	39.6
10	75.0	72.1	73.1	73.1	72.6	73.5	73.8	75.1	73.5
11	141.1	140.9	141.1	140.6	140.6	43.5	38.8	139.7	142.3
12	170.8	170.5	171.1	170.2	170.5	179.0	179.1	171.7	170.3
13	118.6	118.2	118.8	119.5	118.8	9.7	10.8	118.2	119.2
14	33.0	21.8	30.0	23.6	29.8	27.1	28.5	31.6	27.5
15	18.6	15.8	15.0	15.1	16.6	13.8	14.4	13.0	13.9
1′	72.4	72.3	72.2	72.3	131.8	72.9	72.4	72.8	72.9
2′	39.3	38.7	39.1	39.1	195.9	39.6	39.4	39.5	39.6
3′	125.5	124.8	125.2	125.2	135.8	125.4	125.3	124.5	125.4
4′	140.6	140.6	141.0	141.1	170.2	140.8	140.4	141.1	140.8
5′	53.0	53.1	52.0	52.1	53.8	53.8	54.0	53.5	53.9
6′	82.2	81.7	80.0	79.8	83.0	83.2	82.8	82.3	83.2
7′	54.0	56.9	52.5	52.6	59.2	52.4	52.8	49.8	52.5
8′	22.7	21.2	21.4	21.6	25.3	22.6	21.0	23.7	22.8
9′	33.4	33.6	32.6	32.7	38.8	33.4	34.3	33.6	33.4
10′	62.4	62.5	62.1	62.0	152.0	63.4	62.6	63.4	63.5
11′	56.8	56.7	57.4	57.5	56.6	55.5	55.7	54.9	55.6
12′	184.8	182.2	179.0	178.4	180.2	186.2	185.6	183.8	186.1
13′	43.9	40.7	35.5	34.8	41.6	35.5	35.1	34.7	35.4
14′	22.6	21.3	22.6	22.7	21.4	22.8	22.4	22.8	22.8
15′	18.8	17.4	18.8	18.8	20.2	18.9	18.5	18.6	18.9

[a]Recorded in $CDCl_3$. [b]Recorded in CD_3OD. [c]Recorded at 150 MHz. [d]Recorded at 100 MHz.

Fig. 8C, the expression of CYCLINB1 and CDC2 were suppressed with increasing concentration of compound **12** (0.0, 2.0, 4.0, and 6.0 μmol/L). Furthermore, the apoptosis effects on HepG2 cells were detected by flow cytometry. Compared to the control cells, increasing concentration of compound **12** led to enhancement in the apoptotic effect varying from 17.2% (2.0 μmol/L) to 35.9% (4.0 μmol/L), and 65.0% (8.0 μmol/L) as displayed in Fig. 9. Annexin V and propidium iodide (Annexin V/PI) double staining revealed that compound **12** induced accumulation of cells in early- (Annexin V+/PI−) and late-stage (Annexin V+/PI+) apoptosis in a dose dependent manner. Moreover, the level of apoptosis-related proteins BCL-2 and PARP-1 which are indicators of apoptosis was estimated by using western blot assay. The results indicated that compound **12** down-regulated the expression of BCL-2 and PARP-1 in a dose-dependent manner and activated PARP-1 to up-regulate the expression of cleaved-PARP-1. Thus, these results suggested that compound **12** inhibited the growth of HepG2 cells through arresting the cells cycle in G2/M phase and inducing cell apoptosis. In Ye's paper[42], lavandiolide H (**12**) did not showed any anti-inflammatory activity. Even through lavandiolide H (**12**) was reported in Ye's paper, our manuscript first reported the cytotoxicity and preliminary mechanism of lavandiolide H (**12**).

3. Conclusions

In summary, 18 new guaianolide dimers and five known compounds lavandiolides A (**3**), B (**4**), C (**23**), H (**12**), and J (**9**) with a spiro-system composed of two monomeric sesquiterpene lactone units were isolated and identified from *A. atrovirens* guided by cytotoxicity against HepG2 cell line. Their structures were elucidated based on extensive analyses of NMR spectroscopic data, X-ray analyses, and ECD spectra. Structurally, these compounds were involved in seven different kinds of connecting model. Five compounds showed higher activities against HepG2 cells with IC_{50} values superior to sorafenib, three compounds exhibited cytotoxicity against SMMC-7721 cells with IC_{50} values better than sorafenib, and seven compounds showed

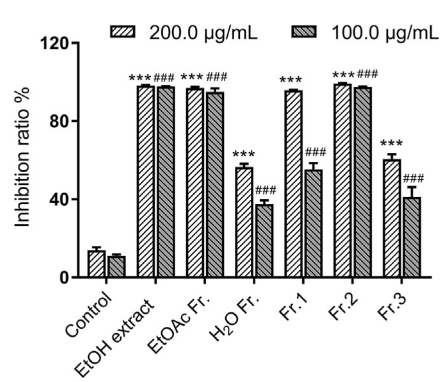

Figure 6 Cytotoxic activities of the EtOH extract and each fraction of *A. atrovirens* against HepG2 cells at 200.0 and 100.0 μg/mL. Sorafenib with an IC_{50} value of 6.0 μg/mL was used as the positive control. $***P < 0.001$ *versus* the control (200.0 μg/mL) group, $^{###}P < 0.001$ *versus* the control (100.0 μg/mL) group, $n = 3$.

Table 6 Cytotoxicity of compounds **1**−**23** from *A. atrovirens*.

No.	IC_{50} (μmol/L)		
	HepG2	SMMC-7721	Huh7
1	4.4 ± 0.2	9.6 ± 0.3	7.6 ± 0.3
2	35.7 ± 1.0	86.6 ± 4.4	35.1 ± 0.4
3	5.5 ± 0.3	22.5 ± 2.7	5.4 ± 0.4
4	21.1 ± 2.9	85.4 ± 7.0	85.0 ± 3.9
5	3.3 ± 0.8	18.7 ± 1.9	5.7 ± 0.2
6	116.9 ± 4.3	8.9 ± 0.1	4.5 ± 0.2
7	6.0 ± 0.1	43.8 ± 1.4	18.6 ± 0.2
8	12.7 ± 1.9	8.9 ± 0.3	5.9 ± 0.3
9	33.4 ± 6.2	111.9 ± 8.8	70.3 ± 2.6
10	10.3 ± 3.1	24.4 ± 0.2	8.2 ± 0.3
11	58.6 ± 7.2	12.9 ± 0.3	9.1 ± 0.3
12	3.8 ± 0.4	4.6 ± 1.1	4.5 ± 0.1
13	5.3 ± 0.2	17.2 ± 1.3	4.0 ± 0.1
14	7.6 ± 0.2	6.6 ± 0.1	6.9 ± 0.1
15	6.7 ± 0.1	6.0 ± 0.3	5.6 ± 0.2
16	8.8 ± 0.2	24.4 ± 1.3	16.5 ± 0.5
17	19.5 ± 0.8	22.3 ± 0.1	8.4 ± 0.1
18	25.7 ± 2.2	11.4 ± 1.9	16.3 ± 0.1
19	7.1 ± 0.1	75.4 ± 2.3	99.3 ± 7.3
20	13.0 ± 0.3	21.6 ± 2.0	10.4 ± 0.2
21	28.8 ± 0.2	10.1 ± 0.5	16.7 ± 0.5
22	6.4 ± 0.1	47.2 ± 1.3	36.3 ± 0.4
23	33.4 ± 0.9	21.9 ± 0.4	20.6 ± 0.3
Sorafenib	7.7 ± 0.4	9.9 ± 0.8	8.3 ± 0.4

Data were expressed as means ± SD ($n = 3$).

higher potential effects against Huh7 cells with IC_{50} values superior to sorafenib. Notably, four compounds (**1**, **12**, **14**, and **15**) exhibited significant inhibitory activity on the three human hepatoma cell lines, and compound **12** showed the highest activity against three human hepatoma cell lines with IC_{50} values of 3.8, 4.6, and 4.5 μmol/L. The mechanism-of-action investigation revealed that compound **12** dose-dependently inhibited cell migration and invasion, induced G2/M cell cycle arrest and cell apoptosis in HepG2 cells, down-regulated the expression of BCL-2 and PARP-1, and activated PARP-1 to up-regulate the expression of cleaved-PARP-1. Our findings provide a series of new guaianolide dimers as candidate molecules against hepatoma. The synthesis, structure modification, structure−activity relationship, and in-depth mechanism of the active sesquiterpenoid dimers are ongoing in our laboratory, and will be reported in due course.

4. Experimental

4.1. *General experimental procedures*

See Supporting Information.

4.2. *Plant materials*

Artemisia atrovirens Hand.-MaZZ. was collected in July 2018 from Kunming, China, and identified by Professor Dr. Ligong Lei (CAS Key Laboratory for Plant Diversity and Biogeography of East Asia, Kunming Institute of Botany, Chinese Academy of Sciences, China). A voucher specimen (No. 20180716-01) was deposited in the Laboratory of Antivirus and Natural Medicinal Chemistry, Kunming Institute of Botany, Chinese Academy of Sciences, Kunming, China.

4.3. *Extraction and isolation*

The powdered and air-dried *A. atrovirens* (60 kg) was extracted twice with EtOH at room temperature (four days each time). After evaporation of the organic solvent *in vacuo*, the residue was suspended in H_2O and extracted with EtOAc. The EtOAc-soluble fraction (3.4 kg) was subjected to a silica gel column chromatography (Si CC, 17 kg, 30 cm × 145 cm) and eluted with a gradient of acetone−petroleum ether (PE; 10:90 to 100:0, *v*/*v*) to afford three fractions [Fr. 1 (1.0 kg), Fr. 2 (450 g), and Fr. 3 (1.7 kg)]. Fr. 2 (450 g) was separated by silica gel column chromatography (Si CC, 3.6 kg, 20 cm × 45 cm) and eluted with a stepwise gradient of EtOAc−PE (10:90 to 50:50, *v*/*v*) to yield four subfractions (Fr. 2-1−Fr. 2-4). Fr. 2-1 (91 g) was fractionated by MPLC on an MCI gel CHP 20P column (490 g, 5 cm × 50 cm) eluting with a gradient solvent of H_2O−MeOH (50:50, 30:70, 10:90, and 0:100) to provide four subfractions (Fr. 2-1-1−Fr. 2-1-4). Fr. 2-1-3 (26 g) was applied to Si CC (260 g, 6.0 cm × 25 cm) using EtOAc−PE as eluents (10:90 to 40:60) to yield five subfractions (Fr. 2-1-3-1−Fr. 2-1-3-5). Fr. 2-1-3-4

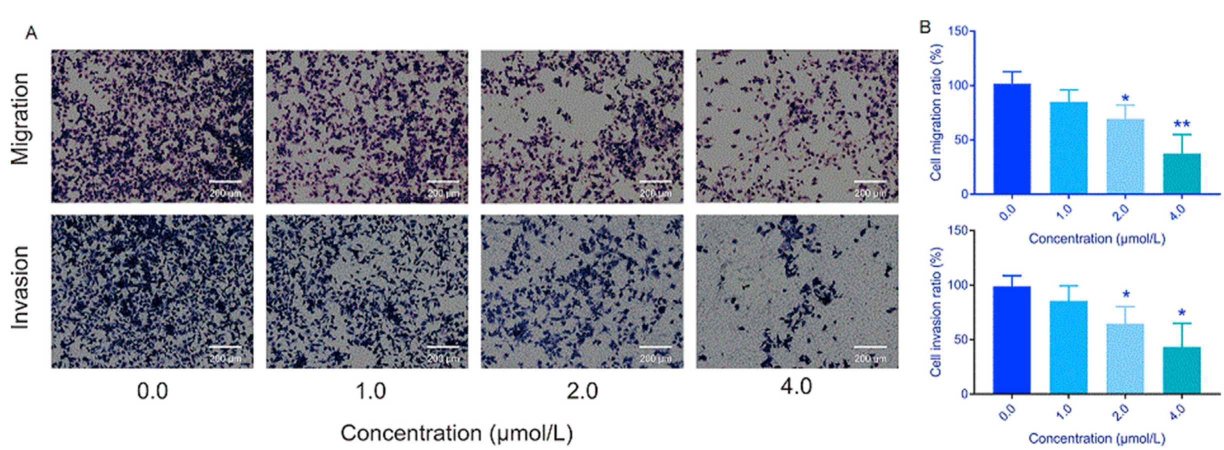

Figure 7 Inhibitory effects of compound **12** on HepG2 cell migration and invasion. HepG2 cells were treated with different concentrations (0.0, 1.0, 2.0 and 4.0 μmol/L) of **12** for 48 h. (A) Representative photographs of Transwell assay showed migrated and invaded cells after incubation. (B) Histogram of migrated and invaded cells after incubation. *$P < 0.05$, **$P < 0.01$, and ***$P < 0.001$, $n = 3$.

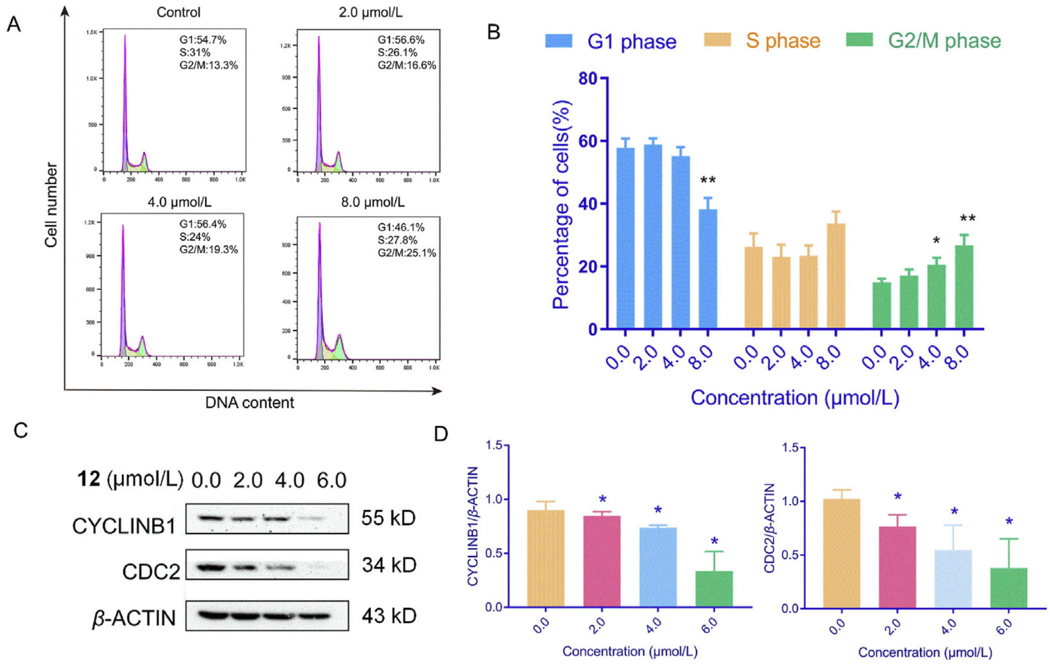

Figure 8 Effects of compound **12** on cell cycle arrest using HepG2 cells. HepG2 cells were treated with different concentrations (0.0, 2.0, 4.0, and 8.0 μmol/L) of **12** for 48 h. (A) and (B) Flow cytometric analysis and cell cycle quantification of HepG2 cells. (C) and (D) Western blot and statistical results of CYCLINB1 and CDC2. *$P < 0.05$, **$P < 0.01$, and ***$P < 0.001$, $n = 3$.

(6.3 g) was chromatographed over Si CC (126 g, 4.5 cm × 25 cm, acetone−PE, 15:85 to 30:70) to produce three subfractions (Fr. 2-1-3-4a–4c). Compound **1** (380 mg) was obtained from Fr. 2-1-3-4b (1.9 g) by recrystallization in MeOH−CH_2Cl_2 (10:90) and the residual part was further purified by preparative HPLC (H_2O−CH_3CN, 44:56, 10.0 mL/min) to yield compounds **2** (13 mg, $t_R = 21.0$ min), **14** (58 mg, $t_R = 32.0$ min), and **21** (11 mg, $t_R = 25.2$ min). Fr. 2-1-3-5 (2.3 g) was separated into three subfractions (Fr. 2-1-3-5a–5c) on Si CC (46 g, 2.5 cm × 25 cm) using a gradient of

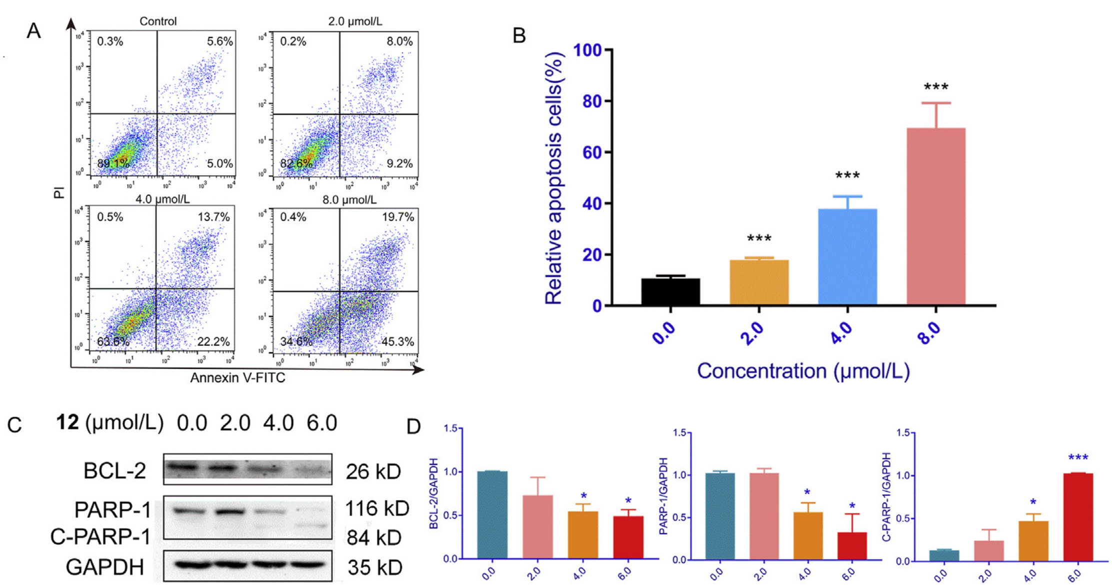

Figure 9 Apoptosis effects of HepG2 cells induced by compound **12**. HepG2 cells were treated with different concentrations (0.0, 2.0, 4.0, and 8.0 μmol/L) of **12** for 48 h. (A) and (B) Flow cytometric analysis and cell apoptosis quantification of HepG2 cells. (C) and (D) Western blot and statistical results of BCL-2, PARP-1, and cleaved-PARP-1. *$P < 0.05$, **$P < 0.01$, and ***$P < 0.001$, $n = 3$.

EtOAc−$CHCl_3$ (2:98 to 10:90). The obtained subfraction Fr. 2-1-3-5a (340 mg) was purified by preparative HPLC (H_2O−CH_3CN, 44:56, 10.0 mL/min) and semi-preparative HPLC (H_2O−MeOH, 20:80, 3.0 mL/min) to afford compounds **7** (14 mg, t_R = 31.5 min), **19** (9 mg, t_R = 23.5 min), **20** (85 mg, t_R = 22.0 min), and **22** (9 mg, t_R = 25.0 min). Compound **15** (45 mg, t_R = 22.0 min) was obtained from Fr. 2-1-3-5b (600 mg) by preparative HPLC separation (H_2O−CH_3CN, 48:52, 10.0 mL/min) and semi-preparative HPLC (H_2O−MeOH, 33:67, 3.0 mL/min). Fr. 2-2 (203.5 g) was separated on an MCI gel CHP 20P column with H_2O−MeOH (50:50, 30:70, 10:90, and 0:100) to provide four subfractions (Fr. 2-2-1–Fr. 2-2-4). Fr. 2-2-2 (39.5 g) was fractionated with Si CC (395 g, 6.0 cm × 40 cm) employing EtOAc−PE (20:80 to 50:50) to give four subfractions (Fr. 2-2-2-1–Fr. 2-2-2-4). Separation of Fr. 2-2-2-2 (7.4 g) on a silica gel column (74 g, 4.0 cm × 20 cm) with acetone−PE (15:85, 20:80, 30:70) gave three fractions (Fr. 2-2-2-2a–2c). Further purification of Fr. 2-2-2-2a by Sephadex LH-20 CC (140 g, 2.5 cm × 175 cm, MeOH−$CHCl_3$, 50:50) followed by preparative TLC (EtOAc–$CHCl_3$, 50:50) yielded compound **6** (24 mg). Fr. 2-2-2-2b (2.8 g) was purified by silica gel CC (EtOAc–$CHCl_3$, 15:85), preparative HPLC (H_2O−CH_3CN, 52:48, 10.0 mL/min), and semipreparative HPLC (H_2O−MeOH, 37:63, 3.0 mL/min) to give compounds **10** (8 mg, t_R = 23.5 min), **11** (5 mg, t_R = 22.7 min), **12** (75 mg, t_R = 31.5 min), and **13** (23 mg, t_R = 29.5 min). Further purification of Fr. 2-2-2-2c (1.4 g) by Sephadex LH-20 CC (120 g, 2.5 cm × 150 cm, MeOH−$CHCl_3$, 50:50) afforded two main fractions (Fr. 2-2-2-2c-1–Fr. 2-2-2-2c-2). Fr. 2-2-2-2c-1 was purified by semipreparative HPLC on an Eclipse XDB-C18 column (H_2O−MeOH, 35:65, 3.0 mL/min) to produce **9** (16 mg, t_R = 27.5 min), **16** (45 mg, t_R = 26.0 min), and **17** (12 mg, t_R = 23.0 min). Semipreparative HPLC purification of Fr. 2-2-2-2c-2 (106 mg) on an Eclipse XDB-C18 column (H_2O−MeOH, 40:60, 3.0 mL/min) yielded **8** (40 mg, t_R = 20.5 min) and **18** (10 mg, t_R = 18.0 min). Fr. 2-2-2-3 (2.5 g) was purified by silica gel CC (acetone–PE, 20:80), preparative HPLC (H_2O−CH_3CN, 45:55, 10.0 mL/min), and semipreparative HPLC (H_2O−CH_3CN, 53:47, 3.0 mL/min) to give compounds **3** (12 mg, t_R = 32.0 min), **4** (74 mg, t_R = 27.3 min), and **5** (75 mg, t_R = 19.8 min), and the residual part was further purified by Sephadex LH-20 CC (48 g, 1.4 cm × 150 cm, MeOH−$CHCl_3$, 50:50) and semi-preparative HPLC (H_2O−CH_3CN, 60:40) to yield compound **23** (13 mg, t_R = 16.7 min).

*4.3.1. Artematrolide A (**1**)*

Colorless orthorhombic crystals (MeOH−CH_2Cl_2, 10:90); mp 239−240 °C; $[\alpha]_D^{25}$ + 29.8 (*c* 0.028, MeOH); IR ν_{max} 3476, 1767, 1744, 1629, 1404, 1257, 1121, 1031 cm^{-1}; CD λ_{max} ($\Delta\varepsilon$) 203 (−0.25), 224 (+1.64), 259 (−0.17) nm; ^1H and ^{13}C NMR data (Tables 1 and 4); (+)-HRESIMS *m/z* 515.2411 $[M+Na]^+$ (Calcd. for $C_{30}H_{36}O_6Na$, 515.2404).

*4.3.2. Artematrolide B (**2**)*

White amorphous powder; $[\alpha]_D^{22}$ + 121.8 (*c* 0.050, MeOH); IR ν_{max} 3510, 3437, 1776, 1755, 1630, 1357, 1256, 1165, 1018 cm^{-1}; CD λ_{max} ($\Delta\varepsilon$) 228 (+0.84), 203 (−0.39) nm; ^1H and ^{13}C NMR data (Tables 1 and 4); (+)-HRESIMS *m/z* 517.2561 $[M+Na]^+$ (Calcd. for $C_{30}H_{38}O_6Na$, 517.2561).

*4.3.3. Artematrolide C (**5**)*

White amorphous powder; $[\alpha]_D^{23}$ + 55.0 (*c* 0.045, MeOH); IR ν_{max} 3450, 1766, 1640, 1440, 1288, 1092 cm^{-1}; CD λ_{max} ($\Delta\varepsilon$) 213 (+0.65), 199 (+0.29) nm; ^1H and ^{13}C NMR data (Tables 1 and 4); (+)-HRESIMS *m/z* 493.2577 $[M+H]^+$ (Calcd. for $C_{30}H_{37}O_6$, 493.2585).

*4.3.4. Artematrolide D (**6**)*

White amorphous powder; $[\alpha]_D^{23}$ + 180.0 (*c* 0.058, MeOH); IR ν_{max} 3449, 1772, 1636, 1439, 1236, 1082, 1009 cm^{-1}; CD λ_{max} ($\Delta\varepsilon$) 213 (+1.06), 200 (+0.51) nm; ^1H and ^{13}C NMR data (Tables 1 and 4); (+)-HRESIMS *m/z* 495.2726 $[M+H]^+$ (Calcd. for $C_{30}H_{39}O_6$, 495.2741).

*4.3.5. Artematrolide E (**7**)*

White amorphous powder; $[\alpha]_D^{22}$ + 48.4 (*c* 0.083, MeOH); UV (MeOH) λ_{max} (log ε) 240 (2.65), 260 (2.59) nm; IR ν_{max} 3446, 1759, 1637, 1384, 1226, 1184 cm^{-1}; CD λ_{max} ($\Delta\varepsilon$) 205 (−0.19), 215 (−0.12), 233 (−0.10), 259 (−0.35) nm; ^1H and ^{13}C NMR data (Tables 1 and 4); (+)-HRESIMS *m/z* 475.2473 $[M+H]^+$ (Calcd. for $C_{30}H_{35}O_5$, 475.2479).

*4.3.6. Artematrolide F (**8**)*

White amorphous powder; $[\alpha]_D^{22}$ + 83.1 (*c* 0.159, MeOH); UV (MeOH) λ_{max} (log ε) 206 (3.30), 231 (2.90), 256 (3.14) nm; IR ν_{max} 3444, 1766, 1687, 1640, 1618, 1321, 1150 cm^{-1}; CD λ_{max} ($\Delta\varepsilon$) 224 (+0.02), 246 (+0.47) nm; ^1H and ^{13}C NMR data (Tables 1 and 4); (+)-HRESIMS *m/z* 491.2413 $[M+H]^+$ (Calcd. for $C_{30}H_{35}O_6$, 491.2428).

*4.3.7. Artematrolide G (**10**)*

Colorless monoclinic crystals (MeOH−CH_2Cl_2, 15:85); mp 200−201 °C; $[\alpha]_D^{21}$ + 77.2 (*c* 0.047, MeOH); IR ν_{max} 3453, 1760, 1653, 1633, 1258, 1055 cm^{-1}; CD λ_{max} ($\Delta\varepsilon$) 214 (+2.18), 255 (−0.13) nm; ^1H and ^{13}C NMR data (Tables 2 and 4); (+)-HRESIMS *m/z* 493.2538 $[M+H]^+$ (Calcd. for $C_{30}H_{37}O_6$, 493.2544).

*4.3.8. Artematrolide H (**11**)*

White amorphous powder; $[\alpha]_D^{25}$ + 37.0 (*c* 0.020, MeOH); IR ν_{max} 3439, 1760, 1632, 1446, 1221, 1061 cm^{-1}; CD λ_{max} ($\Delta\varepsilon$) 198 (−1.09), 211 (−0.22), 222 (−0.75), 265 (+0.13) nm; ^1H and ^{13}C NMR data (Tables 2 and 4); (+)-HRESIMS *m/z* 493.2516 $[M+H]^+$ (Calcd. for $C_{30}H_{37}O_6$, 493.2526).

*4.3.9. Artematrolide I (**13**)*

Colorless monoclinic crystals (MeOH−CH_2Cl_2, 10:90); mp 205−206 °C; $[\alpha]_D^{23}$ + 34.7 (*c* 0.098, MeOH); IR ν_{max} 3440, 1760, 1631, 1443, 1312, 1090 cm^{-1}; CD λ_{max} ($\Delta\varepsilon$) 218 (−0.50), 241 (−0.05) nm; ^1H and ^{13}C NMR data (Tables 2 and 4); (+)-HRESIMS *m/z* 493.2069 $[M+H]^+$ (Calcd. for $C_{30}H_{37}O_6$, 493.2068).

*4.3.10. Artematrolide J (**14**)*

White amorphous powder; $[\alpha]_D^{24}$ + 49.4 (*c* 0.035, MeOH); IR ν_{max} 3446, 1760, 1739, 1631, 1400, 1272, 1133 cm^{-1}; CD λ_{max} ($\Delta\varepsilon$) 208 (+3.75), 229 (−0.27) nm; ^1H and ^{13}C NMR data (Tables 2 and 5); (+)-HRESIMS *m/z* 493.2594 $[M+H]^+$ (Calcd. for $C_{30}H_{37}O_6$, 493.2585).

*4.3.11. Artematrolide K (**15**)*

White amorphous powder; $[\alpha]_D^{23}$ + 17.4 (*c* 0.078, MeOH); IR ν_{max} 3442, 1761, 1631, 1451, 1339, 1177, 1016 cm^{-1}; CD λ_{max} ($\Delta\varepsilon$) 207 (−1.88), 235 (+0.07) nm; ^1H and ^{13}C NMR data (Tables 2 and 5); (+)-HRESIMS *m/z* 493.2550 $[M+H]^+$ (Calcd. for $C_{30}H_{37}O_6$, 493.2561).

*4.3.12. Artematrolide L (**16**)*

White amorphous powder; $[\alpha]_D^{23}$ + 12.0 (*c* 0.063, MeOH); IR ν_{max} 3442, 1763, 1632, 1402, 1221, 1064 cm^{-1}; CD λ_{max} ($\Delta\varepsilon$) 196 (+1.48), 230 (−0.30) nm; ^1H and ^{13}C NMR data (Tables 2 and 5); (+)-HRESIMS *m/z* 493.2583 $[M+H]^+$ (Calcd. for $C_{30}H_{37}O_6$, 493.2585).

*4.3.13. Artematrolide M (**17**)*

White amorphous powder; $[\alpha]_D^{25}$ + 40.2 (*c* 0.115, MeOH); IR ν_{max} 3445, 1766, 1632, 1406, 1344, 1219, 1015 cm^{-1}; CD λ_{max} ($\Delta\varepsilon$) 196 (+1.28), 229 (−0.19) nm; ^1H and ^{13}C NMR data (Tables 3 and 5); (+)-HRESIMS *m/z* 493.2551 $[M+H]^+$ (Calcd. for $C_{30}H_{37}O_6$, 493.2561).

*4.3.14. Artematrolide N (**18**)*

White amorphous powder; $[\alpha]_D^{23}$ + 38.4 (*c* 0.083, MeOH); UV (MeOH) λ_{max} (log ε) 232 (2.93), 256 (3.12) nm; IR ν_{max} 3441, 1762, 1686, 1638, 1618, 1219, 1146 cm^{-1}; CD λ_{max} ($\Delta\varepsilon$) 212 (−1.62), 239 (+0.39) nm; ^1H and ^{13}C NMR data (Tables 3 and 5); (+)-HRESIMS *m/z* 491.2435 $[M+H]^+$ (Calcd. for $C_{30}H_{35}O_6$, 491.2428).

*4.3.15. Artematrolide O (**19**)*

Colorless orthorhombic crystals (MeOH−CH_2Cl_2, 10:90); mp 195−196 °C; $[\alpha]_D^{22}$ + 32.5 (*c* 0.055, MeOH); IR ν_{max} 3498, 1775, 1721, 1677, 1632, 1329, 1261, 1153 cm^{-1}; CD λ_{max} ($\Delta\varepsilon$) 199 (−3.81), 222 (+1.63) nm; ^1H and ^{13}C NMR data (Tables 3 and 5); (+)-HRESIMS *m/z* 517.2558 $[M+Na]^+$ (Calcd. for $C_{30}H_{38}O_6Na$, 517.2561).

*4.3.16. Artematrolide P (**20**)*

Colorless orthorhombic crystals (MeOH−$CHCl_3$, 15:85); mp 190−192 °C; $[\alpha]_D^{24}$ + 88.7 (*c* 0.030, MeOH); IR ν_{max} 3498, 1783, 1728, 1655, 1632, 1383, 1242, 1037 cm^{-1}; CD λ_{max} ($\Delta\varepsilon$) 198 (−1.04), 217 (+1.30) nm; ^1H and ^{13}C NMR data (Tables 3 and 5); (+)-HRESIMS *m/z* 517.2556 $[M+Na]^+$ (Calcd. for $C_{30}H_{38}O_6Na$, 517.2561).

*4.3.17. Artematrolide Q (**21**)*

Colorless orthorhombic crystals (MeOH−$CHCl_3$, 5:95); mp 190−191 °C; $[\alpha]_D^{23}$ − 87.3 (*c* 0.063, MeOH); IR ν_{max} 3486, 1762, 1751, 1664, 1641, 1386, 1337, 1271 cm^{-1}; CD λ_{max} ($\Delta\varepsilon$) 201 (−3.18), 219 (−0.06), 233 (−0.54), 263 (+0.12) nm; ^1H and ^{13}C NMR data (Tables 3 and 5); (+)-HRESIMS *m/z* 493.2575 $[M+H]^+$ (Calcd. for $C_{30}H_{37}O_6$, 493.2585).

*4.3.18. Artematrolide R (**22**)*

White amorphous powder; $[\alpha]_D^{22}$ + 17.9 (*c* 0.059, MeOH); IR ν_{max} 3499, 1765, 1733, 1668, 1630, 1382, 1294, 1136 cm^{-1}; CD λ_{max} ($\Delta\varepsilon$) 201 (−4.05), 223 (+0.44), 239 (+0.08), 261 (+0.27) nm; ^1H and ^{13}C NMR data (Tables 3 and 5); (+)-HRESIMS *m/z* 515.2405 $[M+Na]^+$ (Calcd. for $C_{30}H_{36}O_6Na$, 515.2404).

4.4. Cytotoxicity assays

See Supporting Information.

4.5. Flow cytometry assays

HepG2 cells were seeded in 6-well plates (2×10^5 cells/well). After adherence, cells were treated with a series of concentrations of **12** (0.0, 2.0, 4.0 and 8.0 μmol/L) for 48 h. Then cells were analyzed in cell flow cytometry assay. In cell cycle assay, cells were collected and fixed in 70% EtOH at −20 °C overnight, washed with PBS, resuspended in PBS containing RNase A (200 μg/mL) for 15 min in 37 °C, and then incubated with propidium iodide (100 μg/mL) for 30 min, and analyzed by flow cytometry subsequently. In apoptosis assay, cells were harvested and suspended in binding buffer, and stained with fluorochrome Annexin V/PI for 15 min. Cell cycle and apoptosis assays were analyzed by using a BD AccuriC6 flow cytometer (BD Biosciences, San Jose, CA, USA)[48].

4.6. Cell migration and invasion assays

In order to evaluate cell migration and invasion, HepG2 cells were analyzed by Transwell assay (Corning, USA). For cell migration assay, HepG2 cells (2×10^5/mL) were suspended and plated on the upper chambers with serum-free DMEM overnight and treated with compound **12** for 48 h. Then, cells in the upper chambers were wiped by cotton swabs, the migrated cells were fixed in 70% ethanol and stained with crystal violet solution (0.1%) for 30 min. The upper chambers were washed with PBS twice and dried. Then, images were taken by imaging system (Olympus IX73)[49].

For cell invasion assay, matrigel was diluted to 1:50 in pre-cool DMEM medium on ice and added to the upper chamber before seeding cells. The subsequent procedures were the same as above.

4.7. Western blot

HepG2 cells were treated with compound **12** for 48 h and lysed in RIPA buffer to extract total protein, and protein concentration was quantified by BCA protein assay kit. Protein samples were separated using SDS-PAGE and transferred to PVDF membrane. The membranes were incubated with specific primary antibodies at 4 °C overnight, subsequently. The membranes were incubated with homologous secondary antibodies and detected by ECL solution (Advansta, USA) and photographed by using multispectral imaging system (UVP, USA)[50].

4.8. Theoretical ECD calculation

The ECD calculations for compounds **2**, **5**−**8**, **11**, **14**−**18**, and **22** were performed with the Gaussian 09 program package. Their relative configurations of those compounds were determined based on their ROESY experiments. Their structures were pre-optimized with MM2 method, and further optimized by the DFT calculation at the b3lyp/6-31G(d,p) level in the gas phase. Frequency calculation was performed at the same level to exclude imaginary frequencies. ECD calculation was performed using the TD-DFT methodology at the b3lyp/6-31G(d,p) level in methanol. Solvent effects were taken into consideration using the SCRF method with the IEFPCM model.

4.9. X-ray crystallographic analyses

Crystals of compounds **1**, **4**, **10**, **12**, **13**, **19**−**21** were obtained by using the solvent vapor diffusion method. The single-crystal X-ray diffraction data were recorded on a Bruker D8 QUEST instrument (Cu Kα radiation). Crystals were kept at 100.(2) K during data collection. The crystallographic data of those compounds in standard CIF format were deposited at the Cambridge Crystallographic Data Centre. The data can be accessed free of charge at http://www.ccdc.cam.ac.uk/.

Crystallographic data for **1**: $C_{30}H_{36}O_6$, M = 492.59, a = 8.9597(2) Å, b = 13.6560(3) Å, c = 20.5728(4) Å, α = 90°, β = 90°, γ = 90°, V = 2517.16(9) Å^3, T = 100.(2) K, space group $P2_12_12_1$, Z = 4, μ(Cu Kα) = 0.722 mm^{-1}, 43,964 reflections measured, 4948 independent reflections (R_{int} = 0.0243). The final R_1 values were 0.0306 [$I > 2\sigma(I)$]. The final $wR(F^2)$ values were 0.1081 [$I > 2\sigma(I)$]. The final R_1 values were 0.0316 (all data). The final $wR(F^2)$ values were 0.1103 (all data). The goodness of fit on F^2 was 1.111. Flack parameter = −0.009(17). CCDC 1999120.

Crystallographic data for **4**: $C_{30}H_{38}O_6$, M = 494.60, a = 9.7182(2) Å, b = 15.6711(3) Å, c = 16.9253(3) Å, α = 90°, β = 94.6810(10)°, γ = 90°, V = 2569.04(9) Å^3, T = 100.(2) K, space group $P1211$, Z = 4, μ(Cu Kα) = 0.708 mm^{-1}, 52,514 reflections measured, 10,083 independent reflections (R_{int} = 0.0307). The final R_1 values were 0.0263 [$I > 2\sigma(I)$]. The final $wR(F^2)$ values were 0.0661 [$I > 2\sigma(I)$]. The final R_1 values were 0.0268 (all data). The final $wR(F^2)$ values were 0.0666 (all data). The goodness of fit on F^2 was 1.051. Flack parameter = 0.04(3). CCDC 1999121.

Crystallographic data for **10**: $C_{30}H_{36}O_6$, M = 492.59, a = 8.7039(2) Å, b = 16.5287(4) Å, c = 9.2353(2) Å, α = 90°, β = 97.9230(10)°, γ = 90°, V = 1315.95(5) Å^3, T = 100.(2) K, space group $P1211$, Z = 2, μ(Cu Kα) = 0.691 mm^{-1}, 24,243 reflections measured, 5160 independent reflections (R_{int} = 0.0243). The final R_1 values were 0.0256 [$I > 2\sigma(I)$]. The final $wR(F^2)$ values were 0.0662 [$I > 2\sigma(I)$]. The final R_1 values were 0.0257 (all data). The final $wR(F^2)$ values were 0.0662 (all data). The goodness of fit on F^2 was 1.061. Flack parameter = 0.07(3). CCDC 1999123.

Crystallographic data for **12**: $2(C_{30}H_{36}O_6)\cdot H_2O$, M = 1003.19, a = 9.2451(3) Å, b = 32.7201(9) Å, c = 9.2897(3) Å, α = 90°, β = 114.6360(10)°, γ = 90°, V = 2554.35(14) Å^3, T = 100.(2) K, space group $P1211$, Z = 2, μ(Cu Kα) = 0.736 mm^{-1}, 47963 reflections measured, 10064 independent reflections (R_{int} = 0.0271). The final R_1 values were 0.0256 [$I > 2\sigma(I)$]. The final $wR(F^2)$ values were 0.0657 [$I > 2\sigma(I)$]. The final R_1 values were 0.0257 (all data). The final $wR(F^2)$ values were 0.0657 (all data). The goodness of fit on F^2 was 1.054. Flack parameter = 0.040(18). CCDC 2004025.

Crystallographic data for **13**: $C_{30}H_{36}O_6$, M = 492.59, a = 16.5004(4) Å, b = 8.9087(2) Å, c = 18.6173(4) Å, α = 90°, β = 108.0790(10)°, γ = 90°, V = 2601.58(10) Å^3, T = 100.(2) K, space group $P1211$, Z = 4, μ(Cu Kα) = 0.699 mm^{-1}, 57,080 reflections measured, 10,194 independent reflections (R_{int} = 0.0603). The final R_1 values were 0.0400 ($I > 2\sigma(I)$). The final $wR(F^2)$ values were 0.1029 ($I > 2\sigma(I)$). The final R_1 values were 0.0407 (all data). The final $wR(F^2)$ values were 0.1037 (all data). The goodness of fit on F^2 was 1.035. Flack parameter = 0.03(6). CCDC 2042988.

Crystallographic data for **19**: $C_{30}H_{38}O_6$, M = 494.60, a = 8.8693(2) Å, b = 13.6784(3) Å, c = 21.2902(5) Å, α = 90°, β = 90°, γ = 90°, V = 2582.88(10) Å^3, T = 100.(2) K, space group $P2_12_12_1$, Z = 4, μ(Cu Kα) = 0.704 mm^{-1}, 48,650 reflections measured, 5081 independent reflections (R_{int} = 0.0251). The final R_1 values were 0.0265 [$I > 2\sigma(I)$]. The final $wR(F^2)$ values were 0.0688 [$I > 2\sigma(I)$]. The final R_1 values were 0.0266 (all data). The final $wR(F^2)$ values were 0.0689 (all data). The goodness of fit on F^2 was 1.048. Flack parameter = −0.003(17). CCDC 1999124.

Crystallographic data for **20**: $C_{30}H_{38}O_6\cdot CHCl_3$, M = 613.97, a = 10.4221(3) Å, b = 12.2544(3) Å, c = 23.5810(6) Å, α = 90°, β = 90°, γ = 90°, V = 3011.68(14) Å^3, T = 100.(2) K, space group $P2_12_12_1$, Z = 4, μ(Cu Kα) = 3.102 mm^{-1}, 54935 reflections measured, 5892 independent reflections (R_{int} = 0.0346). The final R_1 values were 0.0285 [$I > 2\sigma(I)$]. The final $wR(F^2)$ values were 0.0754 [$I > 2\sigma(I)$]. The final R_1 values were 0.0286 (all data). The final $wR(F^2)$ values were 0.0755 (all data). The goodness of fit on F^2 was 1.067. Flack parameter = 0.045(3). CCDC 1999125.

Crystallographic data for **21**: $C_{30}H_{36}O_6$, M = 492.59, a = 8.9299(2) Å, b = 13.2860(4) Å, c = 21.1616(6) Å, α = 90°, β = 90°, γ = 90°, V = 2510.67(12) Å^3, T = 100.(2) K, space group $P2_12_12_1$, Z = 4, μ(Cu Kα) = 0.724 mm^{-1}, 24592 reflections measured, 4932 independent reflections (R_{int} = 0.0367). The final R_1 values were 0.0361 [$I > 2\sigma(I)$]. The final $wR(F^2)$ values were 0.0943 [$I > 2\sigma(I)$]. The final R_1 values were 0.0362 (all data). The final $wR(F^2)$ values were 0.0944 (all data). The goodness of fit on F^2 was 1.065. Flack parameter = 0.05(3). CCDC 1999126.

Acknowledgments

This study was supported by the Yunnan Wanren Project (YNWR-KJLJ-2019-002), and the Program of Yunling Scholarship (Ji-Jun, Chen), the Reserve Talents of Young and Middle-aged Academic and Technical Leaders in Yunnan Province (Changan, Geng).

Author contributions

Ji-Jun Chen designed and guided all the experiments and revised the manuscript. Lihua Su conducted the separation, structural identification, and wrote the manuscript. Xintian Zhang performed the mechanism experiments. Yunbao Ma and Xiaoyan Huang carried out cytotoxicity assays. Changan Geng conducted the ECD calculations and revised the manuscript. Jing Hu designed the pharmacological test and analyzed the corresponding data. Tianze Li doublechecked the data and revised the manuscript. Shuang Tang, Cheng Shen and Zhen Gao participated datum analysis. Xuemei Zhang assisted the chemical experiments. All authors read and approved the final manuscript.

Conflicts of interest

The authors have no conflicts of interest to declare.

Appendix A. Supporting information

Supporting information to this article can be found online at https://doi.org/10.1016/j.apsb.2020.12.006.

References

1. Yang JD, Roberts LR. Hepatocellular carcinoma: a global view. *Nat Rev Gastroenterol Hepatol* 2010;**7**:448−58.
2. Liu YY, Wang W, Fang B, Ma FY, Zheng Q, Deng PY, et al. Antitumor effect of germacrone on human hepatoma cell lines through inducing G2/M cell cycle arrest and promoting apoptosis. *Eur J Pharmacol* 2013;**698**:95−102.
3. Poupon R, Fartoux L, Rosmorduc O. Therapeutic advances in hepatocellular carcinoma. *Bull Acad Natl Med* 2008;**192**:23−31.
4. Chai FN, Ma WY, Zhang J, Xu HS, Li YF, Zhou QD, et al. Coptisine from *Rhizoma coptidis* exerts an anti-cancer effect on hepatocellular carcinoma by up-regulating miR-122. *Biomed Pharmacother* 2018;**103**:1002−11.
5. Gan L, Liu ZJ, Sun C. Obesity linking to hepatocellular carcinoma: a global view. *Biochim Biophys Acta, Rev Cancer* 2018;**1869**:97−102.
6. Zhan ZJ, Ying YM, Ma LF, Shan WG. Natural disesquiterpenoids. *Nat Prod Rep* 2011;**28**:594−629.
7. Zhang R, Tang CP, Liu HC, Ren YM, Ke CQ, Yao S, et al. Tetramerized sesquiterpenoid ainsliatetramers A and B from *Ainsliaea fragrans* and their cytotoxic activities. *Org Lett* 2019;**21**:8211−4.
8. Wang Y, Shen YH, Jin HZ, Fu JJ, Hu XJ, Qin JJ, et al. Ainsliatrimers A and B, the first two guaianolide trimers from *Ainsliaea fulvioides*. *Org Lett* 2008;**10**:5517−20.
9. Xie YG, Zhong XL, Xiao YZ, Zhu SL, Muhammad I, Yan SK, et al. Vieloplains A−G, seven new guaiane-type sesquiterpenoid dimers from *Xylopia vielana*. *Bioorg Chem* 2019;**88**:102891.
10. Hilmi F, Gertsch J, Bremner P, Valovic S, Heinrich M, Sticher O, et al. Cytotoxic *versus* anti-inflammatory effects in HeLa, Jurkat T and human peripheral blood cells caused by guaianolide-type sesquiterpene lactones. *Bioorg Med Chem* 2003;**11**:3659−63.
11. Rozenblat S, Grossman S, Bergman M, Gottlieb H, Cohen Y, Dovrat S. Induction of G2/M arrest and apoptosis by sesquiterpene lactones in human melanoma cell lines. *Biochem Pharmacol* 2008;**75**:369−82.
12. Xue GM, Zhu DR, Zhu TY, Wang XB, Luo JG, Kong LY. Lactone ring-opening *seco*-guaianolide involved heterodimers linked *via* an ester bond from *Artemisia argyi* with NO inhibitory activity. *Fitoterapia* 2019;**132**:94−100.
13. Lindenmeyer MT, Hrenn A, Kern C, Castro V, Murillo R, Mueller S, et al. Sesquiterpene lactones as inhibitors of IL-8 expression in HeLa cells. *Bioorg Med Chem* 2006;**14**:2487−97.
14. Ma LF, Chen YL, Shan WG, Zhan ZJ. Natural disesquiterpenoids: An update. *Nat Prod Rep* 2020;**37**:999−1030.
15. Ling YR, Humphries CJ, Gilbert MG. Artemisia Linnaeus, Sp. P1. 2: 845. 1753. In: Wu ZY, Peter HR, Hong DY, editors. *Flora of China*. 1st ed., vols. 20−21. St. Louis: Science Press: Beijing and Missouri Botanical Garden Press; 2011. p. 676−737.
16. Mohamed AE-HH, El-Sayed MA, Hegazy ME, Helaly SE, Esmail AM, Mohamed NS. Chemical constituents and biological activities of *Artemisia herba-alba*. *Rec Nat Prod* 2010;**4**:1−25.
17. Lee SH, Lee MY, Kang HM, Han DC, Son KH, Yang DC, et al. Antitumor activity of the farnesyl-protein transferase inhibitors arteminolides, isolated from *Artemisa*. *Bioorg Med Chem* 2003;**11**:4545−9.
18. Xue GM, Han C, Chen C, Li LN, Wang XB, Yang MH, et al. Artemisians A−D, diseco-guaianolide involved heterodimeric [4+2] adducts from *Artemisia argyi*. *Org Lett* 2017;**19**:5410−3.
19. Wong HF, Brown GD. Dimeric guaianolides and a fulvenoguaianolide from *Artemisia myriantha*. *J Nat Prod* 2002;**65**:481−6.
20. Wen J, Shi HM, Xu ZR, Chang HT, Jia CQ, Zan K, et al. Dimeric guaianolides and sesquiterpenoids from *Artemisia anomala*. *J Nat Prod* 2010;**73**:67−70.
21. Bohlmann F, Ang W, Trinks C, Jakupovic J, Huneck S. Dimeric guaianolides from *Artemisia sieversiana*. *Phytochemistry* 1985;**24**:1009−15.
22. Huang ZS, Pei YH, Liu CM, Lin S, Tang J, Huang DS, et al. Highly oxygenated guaianolides from *Artemisia dubia*. *Planta Med* 2010;**76**:1710−6.
23. Beauhaire J, Fourrey JL, Vuilhorgne M, Lallemand JY. Dimeric sesquiterpene lactones: Structure of absinthin. *Tetrahedron Lett* 1980;**21**:3191−4.
24. Lee SH, Kim MJ, Bok SH, Lee H, Kwon BM, Shin J, et al. Arteminolide, an inhibitor of farnesyl transferase from *Artemisia sylvatica*. *J Org Chem* 1998;**63**:7111−3.
25. Lee SH, Kim HK, Seo JM, Kang HM, Kim JH, Son KH, et al. Arteminolides B, C, and D, new inhibitors of farnesyl protein transferase from *Artemisia argyi*. *J Org Chem* 2002;**67**:7670−5.
26. Reinhardt JK, Klemd AM, Danton O, De Mieri M, Smiesko M, Huber R, et al. Sesquiterpene lactones from *Artemisia argyi*: absolute configuration and immunosuppressant activity. *J Nat Prod* 2019;**82**:1424−33.
27. Xue GM, Zhu DR, Han C, Wang XB, Luo JG, Kong LY, Artemisianins A−D. New stereoisomers of *seco*-guaianolide involved heterodimeric [4+2] adducts from *Artemisia argyi* induce apoptosis *via* enhancement of endoplasmic reticulum stress. *Bioorg Chem* 2019;**84**:295−301.
28. Karimov Z, Kasymov SZ, Yagudaev MR, Sidyakin GP. Crystal structure of the sesquiterpene lactone absinthin. *Khim Prir Soedin* 1980:729−30.
29. Beauhaire J, Fourrey JL, Lellemand JY, Vuilhorgne M. Dimeric sesquiterpene lactone. Structure of isoabsinthin. Acid isomerization of absinthin derivatives. *Tetrahedron Lett* 1981;**22**:2269−72.
30. Beauhaire J, Fourrey JL, Guittet E. Structure of absintholide, a new guaianolide dimer of *Artemisia absinthium* L. *Tetrahedron Lett* 1984;**25**:2751−4.
31. Ovezdurdyev A, Abdullaev ND, Yusupov MI, Kasymov SZ. Artenolide, a new disesquiterpenoid from *Artemisia absinthium*. *Khim Prir Soedin* 1987;**1987**:667−71.
32. Turak A, Shi SP, Jiang Y, Tu PF. Dimeric guaianolides from *Artemisia absinthium*. *Phytochemistry* 2014;**105**:109−14.
33. Jakupovic J, Chen ZL, Bohlmann F. Artanomaloide, a dimeric guaianolide and phenylalanine derivatives from *Artemisia anomala*. *Phytochemistry* 1987;**26**:2777−9.
34. Tu PF, Wen J, Jiang Y, Zhou SX, inventors, Peking University, assignee. *Guaianolide type sesquiterpene lactones dimers, their preparation and application*. 2009. CN101585841A.
35. Zan K, Chai XY, Chen XQ, Wu Q, Fu Q, Zhou SX, et al. Artanomadimers A−F: six new dimeric guaianolides from *Artemisia anomala*. *Tetrahedron* 2012;**68**:5060−5.
36. Zhang C, Wang S, Zeng KW, Li J, Ferreira D, Zjawiony JK, et al. Nitric oxide inhibitory dimeric sesquiterpenoids from *Artemisia rupestris*. *J Nat Prod* 2016;**79**:213−23.
37. Zhou XD, Chai XY, Zeng KW, Zhao MB, Jiang Y, Tu PF. Artesin A, a new cage-shaped dimeric guaianolide from *Artemisia sieversiana*. *Tetrahedron Lett* 2015;**56**:1141−3.
38. Ma CM, Nakamura N, Hattori M, Zhu S, Komatsu K. Guaiane dimers and germacranolide from *Artemisia caruifolia*. *J Nat Prod* 2000;**63**:1626−9.
39. Lee SH, Kang HM, Song HC, Lee H, Lee UC, Son KH, et al. Sesquiterpene lactones, inhibitors of farnesyl protein transferase, isolated from the flower of *Artemisia sylvatica*. *Tetrahedron* 2000;**56**:4711−5.
40. Hu JF, Feng XZ. Artselenoide, a new dimeric guaianolide from *Artemisia selengensis*. *Chin Chem Lett* 1998;**9**:829−32.
41. Mallabaev A, Tashkhodzhaev B, Saitbaeva IM, Yagudaev MR, Sidyakin GP. Structure of artelein, a new dimeric lactone from *Artemisia leucodes*. *Khim Prir Soedin* 1986;**1986**:46−52.
42. Wang QQ, Zhang T, Ke CQ, Tang CP, Yao S, Lin LG, Ye Y. Sesquiterpene lactone dimers from *Artemisia lavandulifolia* inhibit interleukin-1β production in macrophages through activating autophagy. *Bioorg Chem* 2020;**105**:104451.
43. Deng WQ, Wang J, Wang X, Li Q, Wang Y. Study on chemical components of essential oils from *Artemisia atrovirens*. *Hubei Agri Sci* 2011;**50**:4062−5.

44. Oikawa H, Tokiwano T. Enzymatic catalysis of the Diels–Alder reaction in the biosynthesis of natural products. *Nat Prod Rep* 2004;**21**:321–52.
45. Wang S, Sun J, Zeng KW, Chen XG, Zhou WQ, Zhang C, et al. Sesquiterpenes from *Artemisia argyi*: Absolute configurations and biological activities. *Eur J Org Chem* 2014;**5**:973–83.
46. Kawazoe K, Tsubouchi Y, Abdullah N, Takaishi Y, Shibata H, Higuti T, et al. Sesquiterpenoids from *Artemisia gilvescens* and an anti-MRSA compound. *J Nat Prod* 2003;**66**:538–9.
47. Xu XK, Ye J, Chen LP, Zhang WD, Yang YX, Li HL. Four new isomeric sesquiterpene lactone dimers from *Carpesium faberi*. *Tetrahedron Lett* 2015;**56**:6381–4.
48. Li X, Kong LM, Yang QH, Duan AZ, Ju XM, Cai BC, et al. Parthenolide inhibits ubiquitin-specific peptidase 7 (USP7), WNT signaling, and colorectal cancer cell growth. *J Biol Chem* 2020;**295**:3576–89.
49. Wang HY, Zhang CY, Xu LT, Zang K, Ning ZY, Zhu XY, et al. Bufalin suppresses hepatocellular carcinoma invasion and metastasis by targeting HIF-1α *via* the PI3K/AKT/mTOR pathway. *Oncotarget* 2016;**7**:20193–208.
50. Yu ZY, Wu FL, Chen L, Xie SQ, Li Q, Wang CJ, et al. ETME, a novel β-elemene derivative, synergizes with arsenic trioxide in inducing apoptosis and cell cycle arrest in hepatocarcinoma cells *via* a p53-dependent pathway. *Acta Pharm Sin B* 2014;**4**:424–9.